2023-05-18

frontiers | Frontiers in Earth Science

TYPE Original Research
PUBLISHED 18 May 2023
DOI 10.3389/feart.2023.1177507

OPEN ACCESS

EDITED BY
Marco Viccaro,
University of Catania, Italy

REVIEWED BY
Lorenzo Borselli,
Instituto de geologia—Universidad Autonoma de San Luis Potosi, Mexico
Hans-Balder Havenith,
University of Liège, Belgium
Maurizio Mulas,
ESPOL Polytechnic University, Ecuador

*CORRESPONDENCE
Symeon Makris,
makris.symeon@gmail.com

RECEIVED 01 March 2023
ACCEPTED 05 May 2023
PUBLISHED 18 May 2023

CITATION
Makris S, Roverato M, Dávila-Harris P, Cole P and Manzella I (2023), Distributed stress fluidisation: Insights into the propagation mechanisms of the Abona volcanic debris avalanche (Tenerife) through a novel method for indurated deposit sedimentological analysis. *Front. Earth Sci.* 11:1177507. doi: 10.3389/feart.2023.1177507

Distributed stress fluidisation: Insights into the propagation mechanisms of the Abona volcanic debris avalanche (Tenerife) through a novel method for indurated deposit sedimentological analysis

Symeon Makris[1,2]*, Matteo Roverato[3,4], Pablo Dávila-Harris[5], Paul Cole[1] and Irene Manzella[1,6]

[1]School of Geography, Earth and Environmental Science, University of Plymouth, Plymouth, United Kingdom, [2]School of Geosciences, University of Edinburgh, Edinburgh, United Kingdom, [3]Department of Earth Sciences, University of Geneva, Geneva, Switzerland, [4]Dipartimento di Scienze Biologiche, Geologiche e Ambientali, Alma Mater Studiorum, Università di Bologna, Bologna, Italy, [5]División de Geociencias Aplicadas, IPICYT, San Luis Potosí, Mexico, [6]Department of Applied Earth Sciences, Faculty of Geo-Information Science and Earth Observation (ITC), University of Twente, Enschede, Netherlands

Introduction: Volcanic debris avalanches mobilise large volumes and achieve long runouts with high destructive potential. However, the propagation processes that generate them are not currently explained by theoretical or numerical models, which are unable to represent deposit observations. Evaluation of the dynamics represented in deposits is therefore vital for constraining su ch models. The Abona volcanic debris avalanche deposit is located on the southern flank of the island of Tenerife, Spain. The deposit exhibits universal microfracturing and cataclasis. Fluidal features such as fluidal mixing of lithological units and diffuse boundaries, and mixed matrix are observed throughout the deposit.

Methods: Field description including sedimentology and facies identification and the evaluation of their distribution have allowed the generation of a new conceptual model for the propagation dynamics of this volcanic debris avalanche, and potentially others with similar properties. The deposit is indurated making the detailed study of its sedimentology difficult, especially clast-size analysis. A novel method utilising structure from motion photogrammetry and photographic sampling was employed.

Results: The universal cataclasis of the material and fluidal features suggest that the lack of a major competent material component allowed the mass to fragment and enabled fluidised granular flow behaviour. It is proposed that shear was periodically distributed throughout the body of the avalanche in chaotic temporary shear networks rearranging according to the instantaneous distribution of the mass. Stress and agitation were not temporally or spatially homogenous during propagation. This is also reflected in the unsystematic erosion of the substrate according to the variable basal shear accommodation.

Discussion: It is proposed that lithological properties are potentially a determining factor for the propagation mechanisms, stress distribution, and consequently the

evolution of a volcanic debris avalanche from the initial collapse to its emplacement. This study highlights the importance of dedicated field examinations of sedimentological, morphological, and structural features for providing constraints for models of volcanic debris avalanche dynamics and the factors dictating them. The novel methodology proposed has the potential of broadening the number of events that can be studied and enhancing the understanding of these complex and hazardous phenomena.

KEYWORDS

volcanic debris avalanche, sedimentology, propagation dynamics, clast-size analysis, indurated, photogrammetry, facies, granular temperature

1 Introduction

Volcanic debris avalanches (VDAs) are large landslide events generated by volcanic edifice flank collapses (Ui, 1983; Siebert, 1984; Shea and van Wyk de Vries, 2008; Roverato and Dufresne, 2021) and are a common occurrence in the history of most volcanoes (Siebert and Roverato, 2021). They mobilise volumes up to tens of km^3, and less often up to hundreds of km^3, with runout distances up to 100 km (Dufresne et al., 2010b). Their runout and volume poses a hazard while they can trigger secondary hazards such as volcanic eruptions, debris flows, and tsunamis on ocean island volcanoes (Siebert, 1984; Leyrit, 2000; van Wyk de Vries and Delcamp, 2015; Di Traglia et al., 2018), making them potentially one of the most destructive phenomena for communities living close to volcanoes (Hürlimann et al., 1999). The scale of the tsunami triggered by the flank failure in Anak Krakatau volcano (Indonesia) in December 2018 highlights the potential of cascading hazards (Walter et al., 2019).

VDAs are characterised by long runouts compared to what is predicted by simple frictional models of a sliding solid block (Legros, 2002). This is a characteristic shared with their non-volcanic equivalent rock avalanches (RAs) in mountainous environments which was first studied by Heim (1932). However, it was only after the 1980 Mount St. Helens VDA (Glicken, 1996) that scientific interest towards VDAs increased, with various studies examining VDA dynamics. Many theories have been proposed to explain the mechanisms that enable VDA and RA long runouts. Nevertheless, no single proposed model can explain the enhanced mobility while being consistent with field observations in all events (reviewed in Davies, 1982; Erismann and Abele, 2001; Hungr, 2002; Legros, 2002; Collins and Melosh, 2003; Friedmann et al., 2006; Manzella and Labiouse, 2008; Davies and McSaveney, 2012). Some of the proposed mechanisms suggest intergranular mediums such as water or steam to explain the phenomenon; however, such evidence is not observed in all long runout deposits (Hewitt et al., 2008). Others imply other auxiliary exotic mechanisms such as a frictional heat-generated basal pseudotachylyte/frictionite layer (Erismann, 1979). Today, propagating VDAs/RAs are considered to behave as dense granular flows where grain interactions are the most important energy dissipation process (Voight et al., 1983; Campbell, 1990; Schneider and Fisher, 1998; Davies and McSaveney, 1999; Makris et al., 2020). However, the mechanisms enabling long runouts remain controversial and unresolved (Legros, 2002; Pollet and Schneider, 2004; Banton et al., 2009; Davies and McSaveney, 2012; Perinotto et al., 2015).

A major factor for the lack of understanding of VDA propagation processes and dynamics results from the difficulty of models and theoretical concepts to interpret and represent field observations of the sedimentology and structure of VDA deposits (VDADs) (Perinotto et al., 2015; Johnson et al., 2016). Due to the rarity of recent events, there is a lack of well-preserved deposits. Older deposits are commonly indurated, preventing the detailed study of sedimentology, and especially clast-size analysis. Scarcity, inaccessibility and complexity of deposits encourage alternative study methods such as analogue (e.g., Iverson et al., 2004; Dufresne, 2012; Yang et al., 2015; Manzella et al., 2016; Hu et al., 2020) and numerical modelling (e.g., Campbell et al., 1995; Thompson et al., 2009; 2010; Davies et al., 2010; Cuomo, 2020) to be employed instead of field investigations. However, any model regarding the propagation and emplacement of VDAs/RAs must be consistent with their morphological, sedimentological and structural features (Cruden and Varnes, 1996; Pudasaini and Hutter, 2007; Shea and van Wyk de Vries, 2008). Propagation is here defined as the flow regime phase of a VDA, and emplacement refers to the final deceleration and deposition of the material (Paguican et al., 2021). Although VDA/RA deposits are complex, detailed study of their internal architecture and sedimentology can provide information regarding their dynamics (Dufresne and Dunning, 2017) as demonstrated by dedicated field studies (including but not limited to Smyth, 1991; Glicken, 1996; Roverato and Capra, 2013; Roverato et al., 2015; Dufresne et al., 2016b; Dufresne and Dunning, 2017; Paguican et al., 2021). These sedimentological studies have contributed to the understanding of propagation and internal processes by examining local variability in sedimentology, clast-size and facies distribution, morphology of deposits and substrate perturbation. Such studies enable the reconstruction of the propagation history (Dufresne et al., 2010b) and defining constraints for the development of models reflecting the dynamics and energetics of VDAs.

Clast-size analysis is a key element of sedimentological studies as it allows the study of the evolution of the deposit sedimentology and composition through the different phases of the propagation and the identification of possible mechanisms, including fragmentation (Dunning, 2004; Crosta et al., 2007; Dufresne and Dunning, 2017). The quantitative examination of clast-size distribution in the deposits can offer evidence regarding the distribution of stresses, as exemplified by the study of Dufresne and Dunning (2017), illustrating the sedimentological signature of zones of magnified shear stress. When a deposit is indurated or lithified, clast-size analysis is not possible using conventional sieving or laser diffraction (Merico et al., 2020). The consolidation of the material in ancient

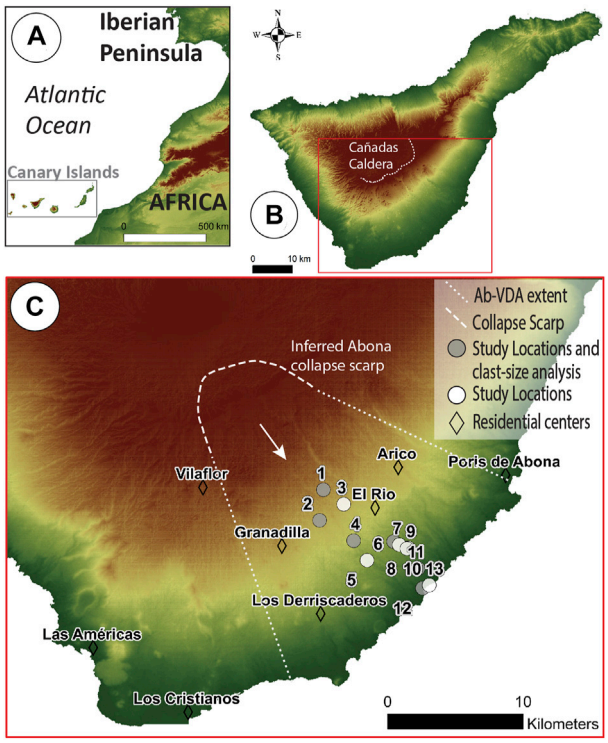

FIGURE 1
(A) The Island of Tenerife with the Cañadas caldera (dotted line); the red rectangle indicates the extent of c. **(B)** Location of the Canary Islands. **(C)** Extent of the Abona volcanic debris avalanche deposit as inferred by Dávila-Harris et al. (2011), with study locations and the locations where sampling for clast-size analysis was carried out.

deposits is suggested by Tost et al. (2014) to have prohibited the study of VDA/RA deposits (Merico et al., 2020). The novel methodology presented in this study allows the clast-size analysis of indurated/lithified deposits. Employment of the proposed methodology in other indurated deposits would extend sedimentological information of VDADs through the addition of more case studies.

This study examines the Abona VDA (Ab-VDA), located in the south of the island of Tenerife, Spain (Figure 1A). Although the deposit is indurated, field observations combined with a novel clast-size analysis methodology allow its examination. The aim is to evaluate the dynamics through assessment of the propagation and emplacement processes that generated the deposit. Analysis of the findings and comparison to other deposits and models aims to ultimately evaluate potential propagation mechanisms that enable the long runouts of VDAs. In order to interpret the deposits, our field investigations generated outcrop maps of the distribution of facies, textures, structures and internal sedimentology (Bernard et al., 2017). The deposit is initially described through its general structure, facies distribution and sedimentological features. The implications of these features for the dynamics of the Ab-VDA in association with other deposits and theoretical and numerical models are also discussed. Finally, this analysis permits the proposal of a new VDA model for the stress accommodation, propagation processes and the formation of the internal architecture and sedimentology which is consistent with the observed structural features and kinematic implications (Shea and van Wyk de Vries, 2008). The findings offer information regarding VDAs which evolve into flows, as well as the factors which might enable such behaviour. The processes suggested offer constraints for conceptual models regarding VDA dynamics and stress distribution.

2 Geological and regional background

2.1 Geological background

Tenerife is the second largest ocean-island volcano on Earth (after Mauna Loa, Hawaii). The island is composed of 90% by volume of a basaltic shield (Hürlimann et al., 1999). This is overlain by the Cañadas stratovolcano, post-shield volcanic complex. This composition reflects the dual, simultaneously active basalt and phonolite magmatic system. Basaltic volcanism began >12 Ma ago and is still active, with the most recent basaltic eruption in 1909 AD (Martí et al., 2010).

The Cañadas edifice is composed of basalt to phonolite lavas and pyroclastic deposits, generated by several eruptive events in the last 3.0–3.8 Ma (Hürlimann et al., 1999; Cas et al., 2022). The evolution of the edifice was characterised by several constructive phases while destructive processes have also been important, with vertical and lateral collapses contributing to the geomorphic evolution of the island (Martí et al., 1997; Martí et al., 2010). Tenerife has hosted large landslides with volumes of 50–500 km^3 and travel distances of up to 100 km (TEIDE GROUP, 1997; Hürlimann et al., 2000; Masson et al., 2002). Large-volume VDAs are responsible for the formation of the major valleys on the flanks of Tenerife between the Upper Pliocene to Middle Pleistocene (Hürlimann et al., 1999; Martí et al., 2010; Dávila-Harris et al., 2011; Cas et al., 2022). The central volcanic complex has hosted major explosive eruptions from the phonolite magma system also generating the present-day Cañadas caldera (Martí et al., 2010). Today, the volcano structure includes the Teide and Pico Viejo stratovolcanoes, and the explosive caldera Cañadas complex (Figure 1B) of >1.8 Ma history with various collapse events (Dávila-Harris et al., 2011; Cas et al., 2022). The current phase corresponds to the constructive phase of the Teide/Pico Viejo complex inside the caldera.

2.2 Abona volcanic debris avalanche—edifice and deposit morphology

The Ab-VDAD was initially classified as a debris flow breccia (Bryan et al., 1998), although later identified as a VDAD by Dávila-Harris et al. (2011). It was generated 733 ± 3 ka ago by a lateral collapse of the Cañadas volcano during an ignimbrite-forming explosive eruption, as supported by petrological evidence and geochronology by Dávila-Harris et al. (2011). The fact that the trigger of the collapse is identified with relative confidence is not common, as most VDADs are difficult to assess with precise time constraints, and even then, triggering mechanisms might have left no evidence in the geological record. The Ab-VDA propagated and was deposited from the Cañadas volcano and towards the southeast, in the region of Abona for at least 21.6 km from the failure scarp

thought to be its source (Figure 1). It covers 90 km^2, and extends further into the ocean (Dávila-Harris et al., 2011). The widespread exposure suggests that the deposit covered the entire region of Abona (Dávila-Harris et al., 2011). The Ab-VDA forms part of the Helecho Formation, which corresponds to the Lower Bandas del Sur Group (Dávila-Harris et al., 2023) and the Guajara Cycle (Cas et al., 2022).

3 Methodology

3.1 Structure and facies mapping

Due to the sedimentological heterogeneity in the Ab-VDAD, detailed facies mapping was necessary prior to sedimentological sampling. At different outcrops the structure, stratigraphy, lithology and other features were identified using the methodology described by Roverato et al. (2015) and Bernard et al. (2017). This allows for targeted sampling along the deposit in specific facies. Initially, the mapping allowed the generation of a structural overview (Bernard and van Wyk de Vries, 2017), identifying outcrops to be sampled for clast-size distribution differences as well as their potential longitudinal evolution along the deposit.

3.2 Clast-size sampling

In this study we have employed a novel combination of techniques and sampling strategies for clast-size analysis of the indurated Ab-VDAD. Size distributions were sampled exclusively for clasts (not matrix) in the MF at seven locations along the deposit (Figure 1C) to evaluate potential longitudinal evolution and variability of clast sizes and proportion of matrix. The method employed was based on manual photographic grid sampling analysis of clasts from scaled orthophotos generated parallel to the outcrop surface (e.g., Ibbeken et al., 1998; Blair and McPherson, 1999; Casagli et al., 2003; Attal and Lavé, 2006; Crosta et al., 2007; Zhang et al., 2015; Ferraro et al., 2018; Harvey et al., 2022).

A frequency-by-area approach methodology was proposed by Chayes (1956) for the mineral composition of cross sections and is based on an area-volume relationship supporting that the ratio of the area occupied by mineral A to the total measurement area is a consistent estimate of the volume percentage of mineral A in the sample (Chayes, 1956, p. 13; Glicken, 1996). This was adopted by Glicken (1996) exclusively for the sampling of the coarse component of samples. The results of the described methodology are different in nature, but theoretically equivalent to the frequency-by-weight output of sieving analysis (Kellerhals and Bray, 1971). Image-based clast-size analysis methods are non-intrusive and provide a more efficient way to extract size distributions of non-cohesive material (Detert and Weitbrecht, 2020) and an alternative in cases where sieving is not an option. Additionally, while sieving methods produce grouped data, photographic analysis produces continuous data which allow more accurate statistical analysis (Buscombe, 2008).

The methodology proposed here utilises photogrammetry, using the commercially available software Agisoft Phtoscan, to combine data from multiple photographs in a single orthophoto sample. Measurements were made on samples at two scales: at the outcrop scale to ensure representation of the coarsest particles from the >1 m scale up to ~ 5 mm, and smaller sample windows for finer particles up to 2 mm. Large-scale samples represent areas up to <32 m^2 and better represent larger clasts, without compromising the resolution of the sample. Conversely, in smaller-scale sample windows (up to ~10 m^2), smaller particles are better represented due to the smaller area represented in every pixel. The resolution achieved by these smaller samples was <0.21 mm/pixel, allowing the sampling of particles up to >0.28 mm. Although the small sample windows had no upper size boundary, due to their small area, they were not suitable for representing larger clasts. Nonetheless, the area represented was up to ~10 m^2 to ensure a sufficient sample size. The results from the two scales were combined to generate the clast-size distribution of the whole size range.

Glicken (1996), as well as other researchers (e.g., Crosta et al., 2007; Shugar and Clague, 2011), have used photographic methods to measure the area occupied by each and every particle over a threshold size in a single photograph to predict the area cover of a particular size range as a proxy for the volume percentage (instead of grid-counting), in accordance with the photo-sieving methodology proposed by Ibbeken and Schleyer (1986). Instead, in the methodology proposed here, the clast-size distribution was determined by grid-sampling individual clasts in an extensive orthophoto sample and calculating the area occupied by each size range. In the environment of the ImageJ software, the desired grid can be generated and geometric properties of clasts can be automatically calculated (Spychala et al., 2021) when their boundaries have been manually drawn (Berends, 2018). Only the particles intersected by grid nodes were measured. The minimum Feret's diameter, defined as the smallest possible distance between two parallel tangents of an object, was used as the size measurement as it can be considered equivalent to the property by which particles are classified when sieved. Where a node was located over matrix, this was noted in the measurements to allow calculation of the percentage of matrix relative to clasts following the methodology described by Blair (1987).

Although this methodology allows the clast-size analysis of the indurated deposit, it is restricted by the limitations of photographic analysis. Therefore, the full size range cannot be sampled because particles smaller than 2 mm could not be accurately and consistently measured. This was especially true of similar-colour particles in the matrix. Additionally, the sedimentological term matrix is an assemblage of smaller particles surrounding coarser particles (Bates and Jackson, 1984), and is therefore, scale-dependent rather than assigning a particular size (Vezzoli et al., 2017). Therefore, a lower boundary had to be established to maintain consistency when comparing matrix-proportion between the samples. For the purposes of this quantitative analysis matrix was considered to be composed of any particle of sand size or finer (<2 mm).

While the area of the large-scale sample orthophotos was generated to cover the largest possible area permitted by the outcrop exposure, and thus include the maximum heterogeneity, the clast sample size, for both the small- and large-scale samples, was chosen according to the guidelines of Bunte and Abt (2001)

FIGURE 2
Section of the outcrop at location 3. The red dashed line represents the boundaries of the deposit thinning against the slope of the paleotopography.

to ensure a <5% error around the mean with confidence of >95%. The calculation of the sample size requirement takes into consideration the median and sorting of the population generated by a pilot sample. One limitation of this methodology is that it does not allow lithological component analysis since lithologies cannot be reliably identified in small particles in the photographic samples. A full evaluation of the methodology, its uncertainties and limitations is included in the Supplementary Appendix S2.

4 Composition, structure and sedimentology of the Ab-VDA

The deposit is exposed across ~10 km from the first outcrop, 11.5 km from the current inferred scarp (location 1) to the coast (location 13) ~22 km from the inferred scarp (Figure 1C). The deposit does not outcrop more proximally than 11.5 km. The thickness of the deposit varies from 2–3 m in some locations up to a maximum thickness of 62 m (at location 4). The Ab-VDAD is predominantly composed of less competent scoria, clasts of ignimbrite lithologies and pumice fall material and substrate-incorporated pumice while it only contains a minor component of lava lithologies (Dávila-Harris et al., 2011). In marginal locations which represent the material deposited near the external boundaries of the avalanche, the deposit thins and disappears on the slopes, illustrating that the avalanche was locally constrained and channelised by ravines in the paleotopography as illustrated in Figure 2. Therefore, at least in some sections, the flow was subdivided into different streams. Six exposed and accessible outcrops have been sampled and studied in terms of clast-size distribution. These locations are illustrated in Figure 1C, with further details in the Supplementary Appendix S1.

4.1 Facies composition and distribution

The deposit is a very poorly sorted, heterolithic breccia which exhibits characteristic VDA block and mixed facies (Dávila-Harris et al., 2011). Here the term edifice block facies (EBF) (equivalent to the block facies of Glicken, 1991) is used instead of block facies. The term was introduced by Bernard et al. (2021) and is here used because only blocks from the original collapsed edifice are observed and no blocks considered to have been incorporated from the propagation path substrate. The term matrix-rich facies (MF) is also used instead of mixed facies (after Roverato et al., 2011) for consistency with the most recent literature. The EBF is composed of undisaggregated or poorly disaggregated portions of the original edifice, and the MF is composed of a heterolithic poorly sorted mixture of clasts and matrix. The facies distribution is chaotic and unsystematic, while outcrops exhibit both facies in proximity. The term matrix refers to finer grains surrounding larger particles (Mehl and Schmincke, 1999), which is scale-dependent rather than assigning a particular size (Vezzoli et al., 2017).

4.1.1 Edifice block facies (EBF)

The Ab-VDAD EBF is composed of unconsolidated, or poorly consolidated, portions of the original edifice (referred to as blocks) emplaced in the deposit unmixed with the surrounding material, retaining lithological distinctness (Bernard et al., 2021). Blocks are universally microfractured and to some degree disaggregated as clasts in their interior are displaced relative to each other. Disaggregation implies the displacement of these components, altering their original relative placement in the structure and fabric of the rock mass. Fracturing refers to the break-up of a block resulting in a fabric of individual component clasts. Lithologies composing blocks include the more competent hydrothermally altered and fresh lavas; the less competent and

10.3389/feart.2023.1177507

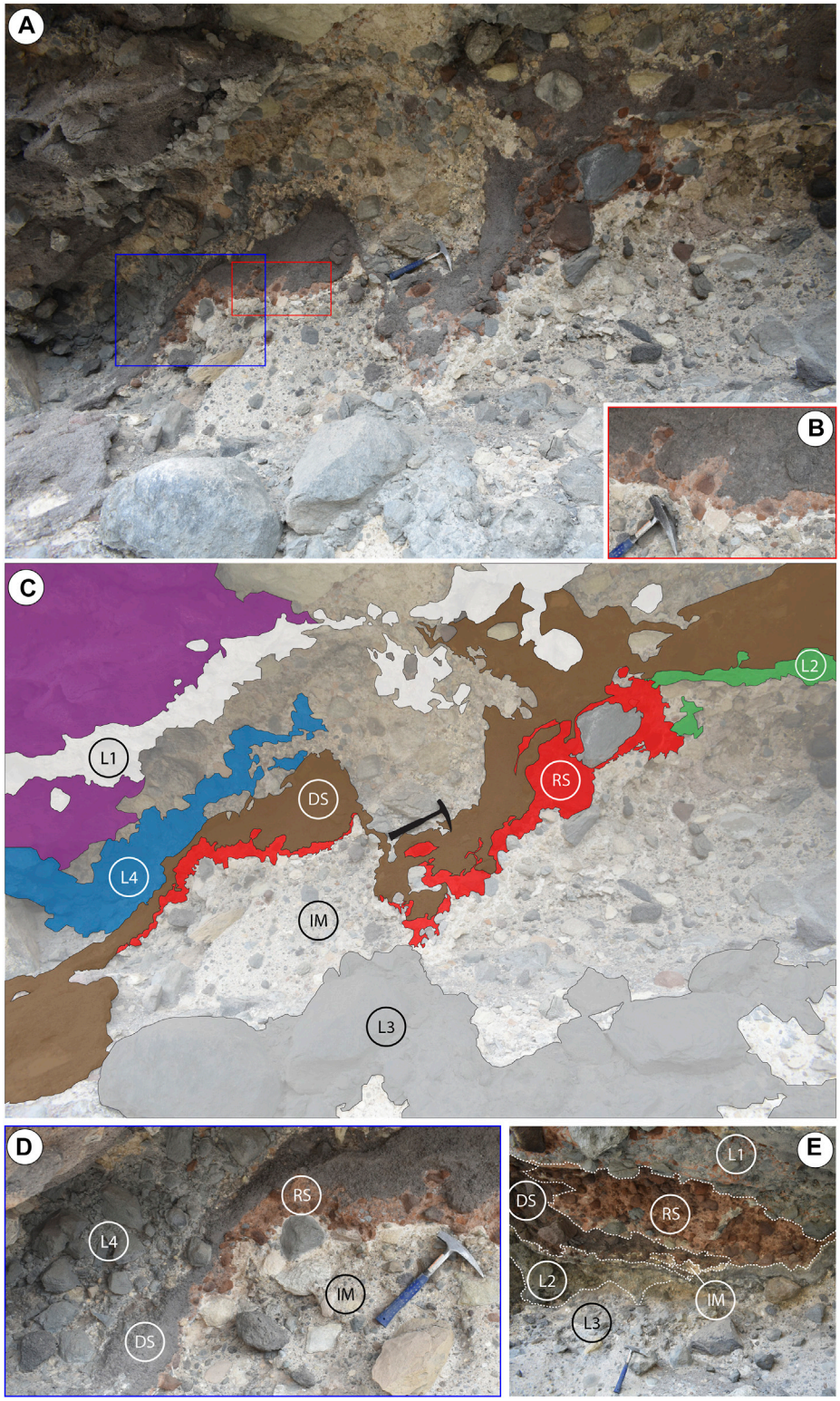

FIGURE 3
Several features from edifice block facies (EBF) of location 2: **(A)** Overview of a characteristic section from this location. Preservation of stretched lithological units as monolithological diamictons. The blue and red rectangles correspond to the extent of d and b respectively. **(B)** Fluidal form intrusion of one unit into another with no mixing. **(C)** The lithological units are here coloured to highlight their fluid-like behaviour, and preservation of stratigraphic sequence. IM, intrablock matrix; L1, lava unit 1; L2, Lava unit 2; L3, Lava unit 3; L4, Lava unit 4; DS, Dark scoria unit; RS, Red scoria unit. **(D)** Lava units and weaker scoria units exhibit different degrees of cataclasis even though they are found in adjacent positions. The lava unit at the left of the image is less comminuted with larger clasts compared to the dark scoria and red scoria units at the centre of the image. **(E)** The lithological units observed in c are here observed at a different area of the same location in a similar stratigraphic sequence.

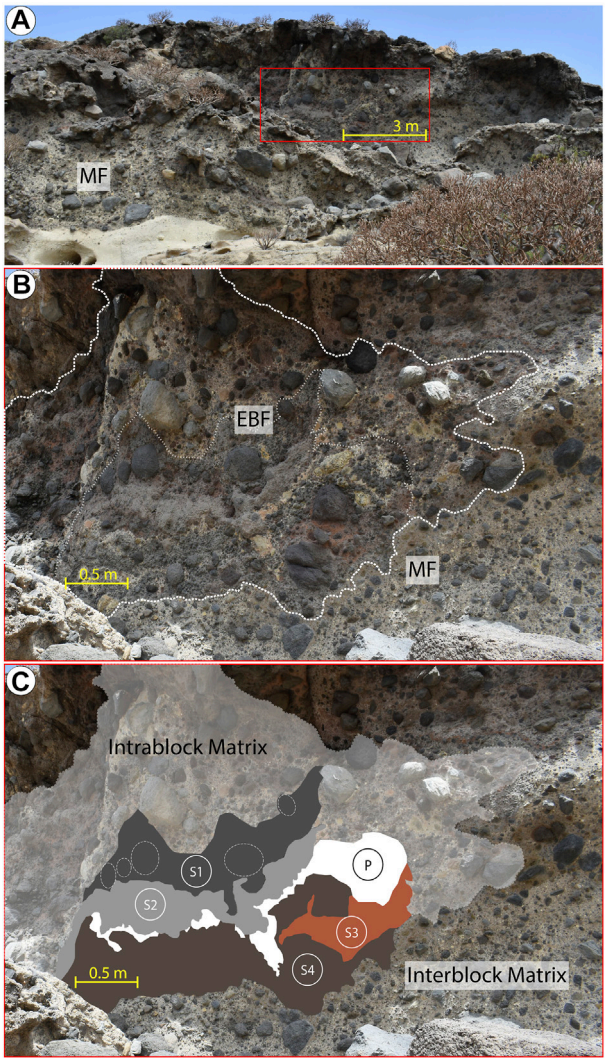

FIGURE 4
The internal structure of the Abona volcanic debris avalanche deposit at location 12. **(A)** The outcrop presents both the matrix-rich facies (MF) as well as the edifice block facies (EBF), and both interblock and intrablock matrix. The area of the red rectangle represents the extent of b and c. **(B)** The bold white dashed line encompasses the EBF which is surrounded by the MF. The contact between the two facies is diffusive. The finer white dashed line encompasses preserved stratigraphic sequence. The boundary between the matrix and the distinct lithological units is also diffusive. **(C)** Same extent as b. The section of preserved stratigraphy is composed of different lithological units of scoria: S1, S2, S3, S4; and pumice: P. Different units have been coloured to highlight their stratigraphic sequence and fluidal mixing. Dashed circles highlight rounded clasts.

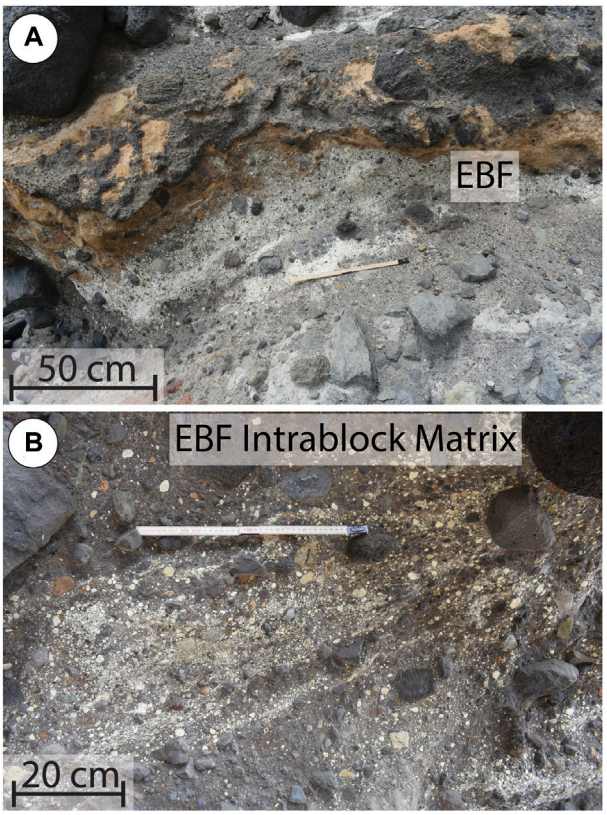

FIGURE 5
(A) Edifice block facies (EBF) from location 3 containing a unit of pumice. **(B)** The intrablock matrix proximal to this unit is enriched in pumice due to the progressive diffusion of material to the matrix.

resistant scoria, ignimbrite and pumice fall lithologies clasts and substrate-incorporated material (Dávila-Harris et al., 2011). However, the proportion of the competent lavas compared to the less competent material is minor throughout the EBF. This is evident at location 2 where the main characteristics of EBF are illustrated in Figure 3. The shape of blocks is distorted and elongated to lenticular shapes, as exemplified by the pumice and scoria units in Figures 3C, D. Nonetheless, blocks retain lithological homogeneity and distinctness compared to surrounding material. Despite the fracturing and distortion, lithological units are preserved in the interior of blocks (Figure 3). Sections of remnant stratigraphic sequence are preserved where these units maintain their original order as illustrated by the sequence of lithological units in Figure 3C. These lithologies are interbedded and stretched to assume fluidal mixing forms (Figures 3B, C). Each unit is composed of a poorly sorted diamicton of monolithological cataclased material. Cataclasis refers to the fracturing, comminution, disaggregation by the displacement of component parts and production of matrix that generates a granular diamicton fabric. Uninterrupted EBF domains extend for more than 100 m; however, undisaggregated portions of remnant stratigraphy are only observed in sections <12 m in length. The EBF with elongated remnant stratigraphic sequence and variable degrees of preservation forms pockets of less disaggregated material in a chaotic deposit where the degree of disaggregation is not systematically distributed. Such remnant stratigraphy is only preserved in pockets within the deposit at locations 5, 12 and 13, as exemplified in Figure 4C illustrating a pocket of EBF and preserved stratigraphy surrounded by MF. The area between undisaggregated blocks is filled by the intrablock matrix as illustrated in Figure 4.

Within the EBF, the intrablock matrix is composed of poorly sorted mixture of heterolithic clasts within a heterolithic matrix. A clast refers to any rock which would not break if passed through a sieve, or was immersed in water, after the definition by Glicken

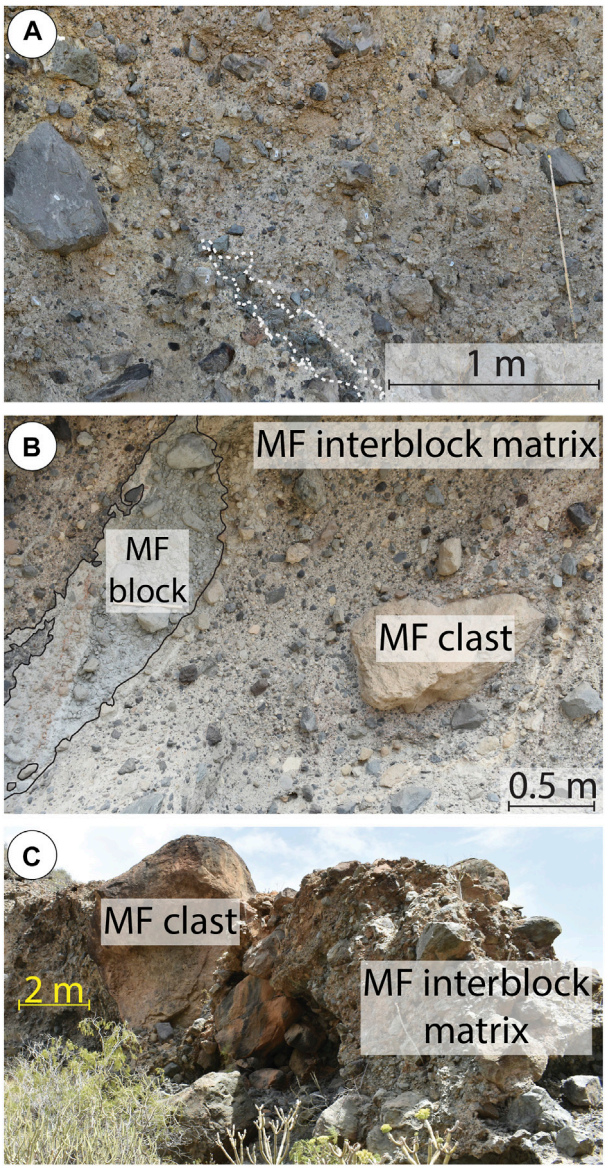

FIGURE 6
(A) Matrix-rich facies in location 2 including a lenticular block with its outline indicated by the dashed white line. This is an orthophoto generated using structure from motion photogrammetry. **(B, C)** illustrate features from location 4. **(B)** A portion of the matrix-rich facies (MF) composed of poorly sorted clasts, interblock matrix as well as a monolithological microfractured block. **(C)** The annotated MF clast is the largest encountered in the deposit and has a maximum diameter of 6 m.

(1991). The lithology of the clasts and matrix represents the lithologies present in the vicinity, within each block. This is evident locally around monolithologic blocks where the nearby matrix is enriched in that lithology. Pumice deposits make this particularly evident, as the nearby matrix has a visibly different composition enriched in the white pumice as illustrated in Figure 5. Here, the intrablock matrix adjacent to a pumice unit is visibly enriched by the diffusing pumice material (Figure 5). The degree of mixing within the intrablock matrix exhibits some variability but is always lower than the interblock matrix, which is completely mixed and heterogeneous in the Ab-VDAD. The intrablock matrix (as well as the intrablock) exhibits no internal structures or features.

4.1.2 Matrix-rich facies (MF)

The MF is exposed in all the locations studied, from the most proximal to the most distal. Its abundance suggests it constitutes the dominant facies component of the deposit although the proportion could not be quantified due to the interrupted exposure. The MF is similar to the equivalent facies reported in other VDADs (e.g., Glicken, 1991; Bernard et al., 2021) and is notably uniform throughout the deposit. The MF consists of a well-mixed, heterolithic, very poorly sorted mixture of subangular-to-subrounded clasts and interblock matrix composed of material from the source edifice (Figures 4, 6A), pumice incorporated from the substrate during propagation (Figure 7), and a small amount of juvenile phonolite clasts. The juvenile clasts have chilled margins and were likely incorporated from a dome collapse (Dávila-Harris et al., 2011). Particles in the MF range from microns up to clasts of <6 m, as shown in Figure 6C. Its composition represents the lithologies that also occur in the EBF. However, a greater degree of mixing and homogenisation produces a distinctive heterolithic matrix which differs from the cataclased but unmixed diamicton of the EBF, as well as the less heterolithic and less mixed intrablock matrix. The difference is illustrated by the comparison of Figure 4B with Figure 6A. The intrablock matrix of Figure 4 is much less poorly sorted, less polylithological and includes a greater proportion of clasts relative to matrix. The percentage of the matrix relative to clasts is highly variable. Although well mixed, the MF also contains a minor quantity of microfractured MF blocks with lenticular shapes (Figures 6A, B and large clasts (e.g. Figure 6C). These represent portions of the original edifice that although included in the MF have not been completely disaggregated. However, the MF lacks any stratification, grading or internal features.

4.2 Internal structure and sedimentology

4.2.1 Fracturing and cataclasis

At the metre and down to the finer than centimetre scale, the material in the EBF is universally fractured and cataclased. The cataclasis of the material generates lithological units composed of larger clasts in a finer matrix assuming the fabric of a diamicton while remaining unmixed and preserving their lithological distinctness as exhibited by different lithological units in Figure 8. Blocks suit the term of fragmental rock clasts used by Alloway et al. (2005) as fractured, deformed blocks in some cases preserving stratigraphic sequence (Figures 3, 4). The products generated by the fracturing and comminution are the particles constituting the intrablock matrix and the MF. Clasts range in roundness from subangular to subrounded and even rounded (e.g., Figure 4, roundness highlighted in Figure 4C). Other than the mentioned microfracturing, and the scarce shear displacement of some larger fractured clasts, no larger-scale brittle deformation, fracturing or faulting has been observed in the Ab-VDAD. In these clast components, displacement is caused by the shear stress parallel to the flow direction generated by differential rates of propagation. Such examples are illustrated in Figures 9A, B.

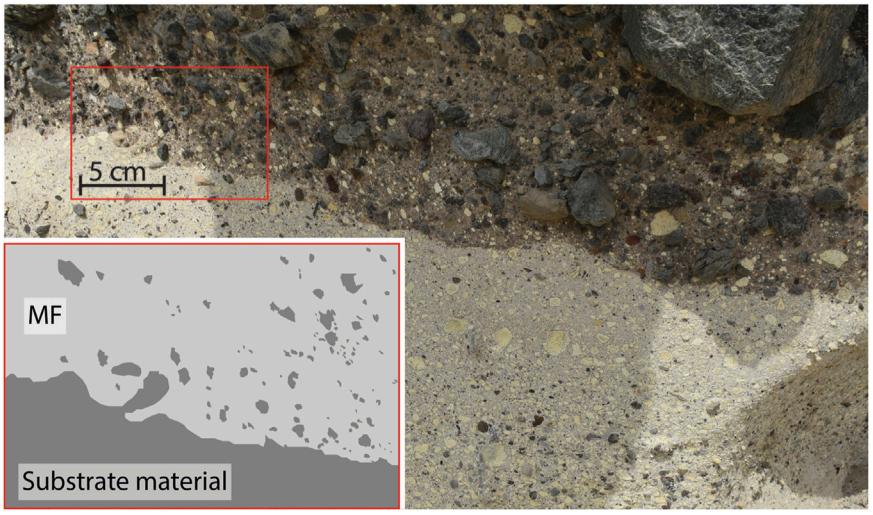

FIGURE 7
Basal contact between the Abona volcanic debris avalanche deposit and the substrate at location 12. The red rectangle represents the extent of the insert at the bottom left of the figure. The insert highlights the incorporation and diffusion of substrate material (dark grey) into the matrix-rich facies (MF) (light grey) due to abrasion.

The degree of fracturing in blocks is not exclusively associated with the distance travelled by the Ab-VDA, as also suggested for other deposits (e.g., Reubi and Hernandez, 2000). The EBF exhibits a variable degree of cataclasis and disaggregation, especially between different lithological components, even at the same outcrop. Qualitative assessment of the Ab-VDAD suggests that less competent lithologies, such as scoria, exhibit more cataclasis than the more competent lavas, as also suggested by Dávila-Harris et al. (2011). The degree of cataclasis varies from pulverized dust to coarse breccias. The differential degree is most obvious where strata composed of competent lava lithologies are in proximity to strata of more cataclased scorias as demonstrated in Figures 3B, D, where parts of the same block, with different lithology exhibit dissimilar degrees of cataclasis and resultant clast sizes. Scoriaceous material, which is weak and porous, is the most strongly cataclased lithology producing a microfractured diamicton composed of clasts in a fine interblock matrix of sand-sized and finer particles, shown in Figure 8C. This style of cataclasis in weaker lithologies has been encountered throughout the Ab-DAD (Figures 3, 4B). In contrast, the more competent lava lithologies, clasts produced are larger and the proportion of matrix is smaller (Figures 3D, 8B).

4.2.2 Fluidal behaviour and features

At the larger outcrop scale, no brittle fracturing or faulting is exhibited. In the EBF, lithological units preserve their distinctness and outline despite assuming distorted thin, elongated, lenticular forms. Where lithologies are interbedded and stretched, they assume fluidal mixing forms where portions of one lithology intrude another unit (Figures 3, 4), preserving their local homogeneity and giving the deposit a form similar to the mixing of viscous fluids as shown in Figure 3C.

Lithological units within the EBF have diffuse boundaries where adjacent to the MF (Figure 10A), or intrablock matrix (Figure 10B). The material from the periphery of a specific unit appears to diffuse outwards from its boundary into the matrix, while gaps created between the diffusing particles are intruded by matrix material. This is illustrated in Figures 10A, B by the lighter-coloured matrix mixing with the darker undisaggregated block material at the boundaries.

Location 12, illustrated in Figure 4A serves as a good example of the internal structure of the Ab-VDAD. This outcrop is composed of MF, which surrounds fractured and partially disaggregated EBF blocks. The contacts between the two facies are diffuse with material from the EBF diffusing into the interblock matrix (Figure 4B). The blocks are composed of elongated lenticular monolithological units with preserved stratigraphic sequence and intrablock matrix (Figure 4C). The mixing of the stratigraphic units illustrates the fluidal behaviour (Figure 4C). Contacts between different units within the block and between the intrablock matrix are also diffusive. The intrablock matrix is composed of the lithologies within the block. Similarly, at location 5 (Figure 3) monolithological units with fluidal features are preserved surrounded by a pumice-rich interblock matrix. Some contacts are not diffusive, but instead, take the form of fluid-like injection of one unit into another, and in the intrablock matrix (Figure 3B).

4.3 Clast-size analysis

Figure 11 illustrates that clasts greater than −9.5φ are only encountered in locations more proximal than 13.05 km (loc. 2). However, other than this observation there is a lack of similarity or evolution with distance in the form of the histograms representing the clast-size distributions of Figure 12. The cumulative plots illustrates in Figure 11A also suggest a lack of systematic clast size variation. Figure 11B illustrates the evolution of the different

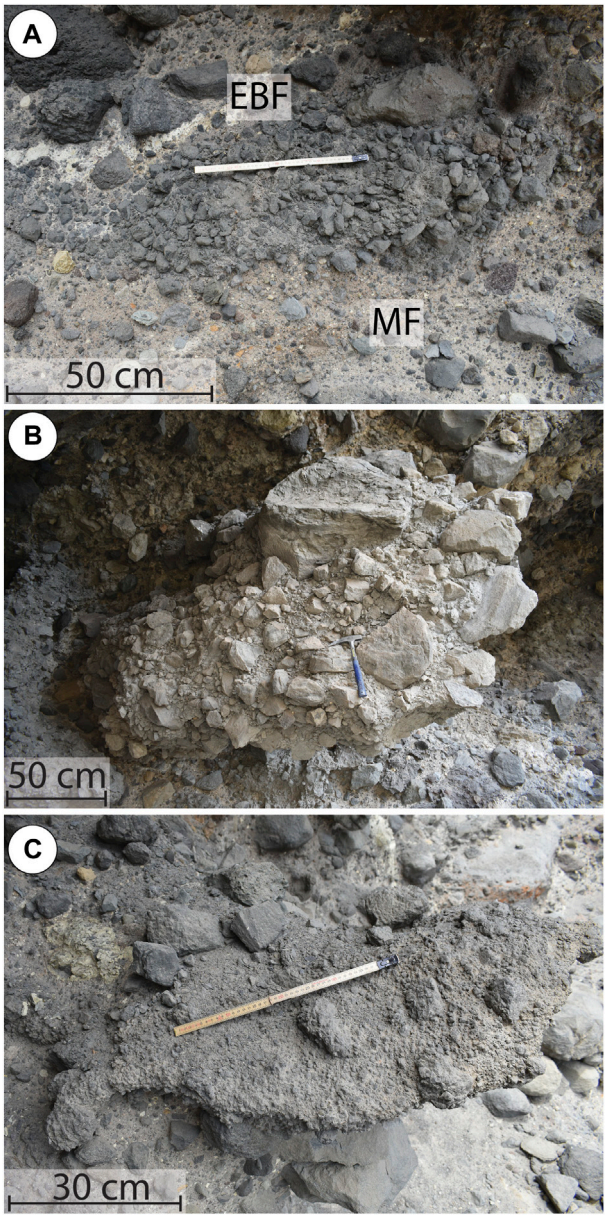

FIGURE 8
Monolithological diamictons. **(A)** Location 6. Cataclased diamicton in contact with the MF, with diffusive boundaries and lenticular shape. **(B)** Location 5. Lava unit exposed in three dimensions due to the preferential erosion of the weaker lithologies around it. The cataclasis generated larger clasts and less matrix in comparison to the other lithologies. **(C)** Block of scoriaceous material at the most distal location 13.

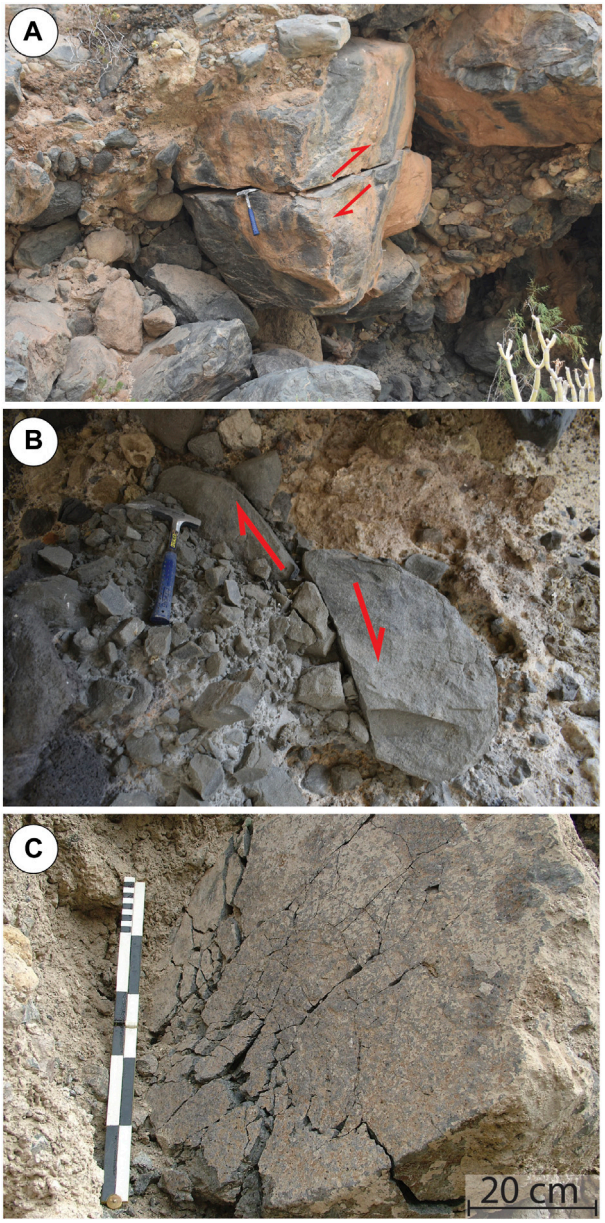

FIGURE 9
Brittle features of the Ab-VDAD. **(A)** Fractured clast with components displaced parallel to the propagation direction (location 4). **(B)** The relative displacement between clasts originating from the same particle illustrates the shear in the material (location 5). **(C)** Fractured block with components preserving their relative position in a jigsaw fabric. This was observed in location 4 but was a rare occurrence for the deposit.

clast-size percentiles along the deposit. P10, P25 and P50 show very little variability. P90 and P75 exhibit a reduction until 17.8 km; however, this trend is subsequently not consistent. Median clast sizes vary between 19 mm and 61.5 mm (Table 1). The clast-size distributions illustrated in Figures 11A, 12, as well as the statistical percentile analysis presented in Figure 11B, illustrate no consistent systematic variation or longitudinal evolution correlated to the distance from the source along the 10 km that the deposit is exposed.

The analysis reveals a variable proportion of matrix between 36% and 65% at different locations of the MF (Table 1). The proportion of matrix is also variable within the same outcrop as illustrated in Table 1 by the two samples carried out for different positions within location 4 (15.67 km from source). This was the tallest outcrop (62 m), presenting high vertical variability in the MF. Sampling was carried out for the matrix at the upper and lower sections of the outcrop (Supplementary Appendix S3). Closer to the base the deposit contains a higher block component, being blockier,

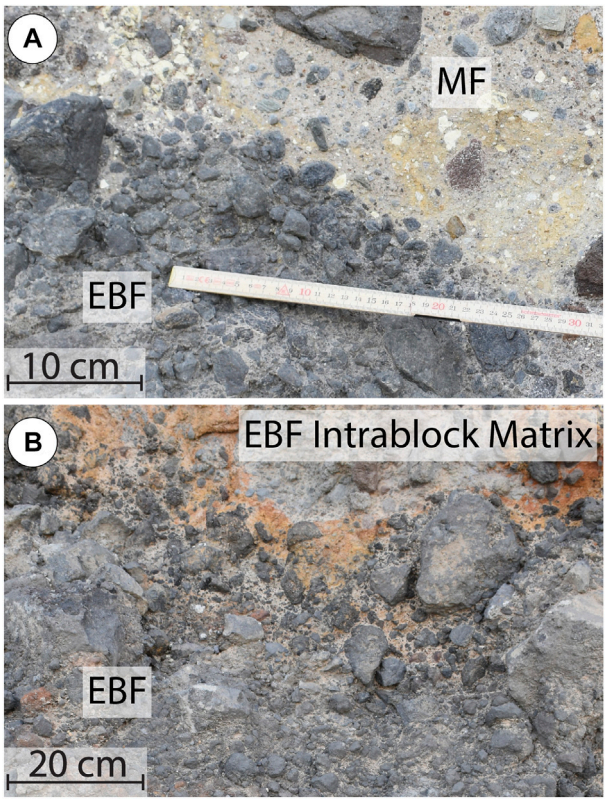

FIGURE 10
Diffusive contact **(A)** between the edifice block facies and the matrix-rich facies; and **(B)** between edifice block facies preserved unmixed lithological unit and intrablock matrix. Both from location 11.

compared to the shallower part of the deposit. The lower sample contains a matrix proportion of 35.6%, while the lower contains 54.7% matrix. The difference is also reflected in a greater mean and median clast size in the lower section compared to the upper (Table 1).

4.4 Substrate interactions

The substrate over which the Ab-VDA propagated is a pumice fall deposit (Moradas Fm.—738 ± 4 ka) in locations more proximal and up to location 10 (Figure 1). In the more distal locations, after location 10, the substrate is the pumice-rich ignimbrite of the Helecho Formation (Cobón Member—733 ± 3 ka) (Dávila-Harris et al., 2011). Between the Moradas formation and the deposit, a thin layer of soil is preserved. The soil represents the brief hiatus in eruptive activity that preceded the Ab-VDA (733 ± 3 ka) (Dávila-Harris et al., 2011). Substrate deformation features observed in the deposit at different locations include bulldozing (where deformed but not incorporated) (Figure 13A), ploughing (where incorporated) (Figure 13B), flame injections (Figure 13C), faulting (Figure 13D) and sharp abrasive erosional contacts (Figure 7). Bulldozing is the pushing and compressing of substrate material into mounds due to the frictional shear of propagating VDA material. Ploughing, on the other hand, is the process whereby the pushed material is detached from the substrate and incorporated en masse (Dufresne et al., 2010a). Substrate incorporation is directly observed at locations that expose the basal contact of the Ab-VDA (e.g., Figure 7), as well as from the existence of pumice from the substrate higher up in the body of the deposit. At the basal contact portions of the substrate have been preserved in the process of being detached as illustrated in Figures 13B–D).

The perturbation of the substrate is highly variable and unsystematic throughout the deposit, even at the metre scale, and there is no systematic variation with distance from the source. Penetration of the substrate occurs by both blocks and matrix. The pumiceous soil layer between the pyroclastic deposits and the deposit is in places preserved (Figures 13E, F), while in others in the same outcrop missing or disturbed (Figure 13F).

5 Discussion

5.1 Internal morphology and sedimentology

5.1.1 Brittle fracturing

All the material in the Ab-VDAD EBF is microfractured and cataclased, with monolithological units assuming the fabric of a diamicton, while highly mixed domains constitute the interblock and intrablock matrix. Undisaggregated material with original textures is almost non-existent in the deposit, despite unfractured and undisaggregated jigsaw blocks being a typical feature of other VDADs (Siebert, 1984; van Wyk De Vries et al., 2001; Makris et al., 2023). Jigsaw-fractured clasts, like the one illustrated in Figure 9C, are few and restricted to specific locations within the deposit. In general, a VDA mass suffers rapid fragmentation and coarse disaggregation at the initial edifice collapse stage (Voight et al., 1983; Glicken, 1991; Longchamp et al., 2016). Nonetheless, in the Ab-VDA, the cataclasis exhibited throughout the deposit (except a minor number of large clasts) suggests syn-propagation progressive fragmentation (Dávila-Harris et al., 2011; Perinotto et al., 2015; Roverato et al., 2015; Paguican et al., 2021) rather than an impulse of fragmentation due to the initial collapse. Syn-propagation fragmentation due to grain-to-grain contact is thought to be generally minimal in VDAs. However, depending on lithology and strength, fragmentation of intact rock can also occur through grain interactions. This has indeed been suggested by Dávila-Harris et al. (2011) for the avalanche and is supported by studies on other VDADs proposing fragmentation as a continuous process, such as Socompa VDA (van Wyk De Vries et al., 2001), Parinacota (Clavero et al., 2002), Taranaki (Roverato et al., 2015) and the study of VDAs of La Réunion Island by Perinotto et al. (2015).

Fragmented particles that do not experience further crushing, but are smoothed and rounded by frictional abrasion in the agitated mass to undergo further size reduction (Schneider and Fisher, 1998; Perinotto et al., 2015; Paguican et al., 2021). In the Ab-VDAD clasts composed of weaker lithologies are locally subrounded-rounded, as illustrated in the examples in Figures 4B, C. Rounded clasts are not a

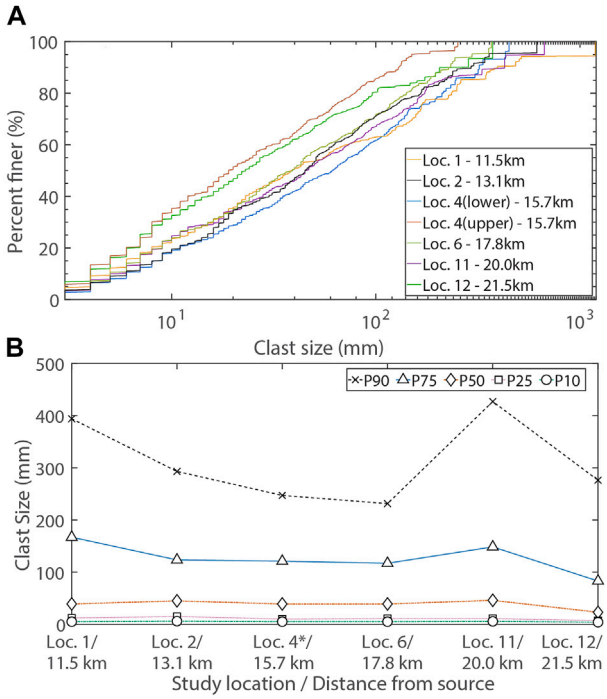

FIGURE 11
Clast size analysis results **(A)** Cumulative plots of the sampled clast populations from all the samples. The legend includes the distance of each location from the source. **(B)** Representation of the 90th, 75th, 50th (median), 35th and 10th percentiles at the different study locations along the deposit. (Note that the upper and lower sections of location 4 are considered together for this plot).

typical feature of VDA/RA deposits. In fact, in RA deposits, composed of more competent material, all clasts are angular due to brittle fractures. Less competent lithologies do rarely exhibit scratching or snubbing of corners in those cases (Hewitt et al., 2008). This feature potentially indicates the weakness of the material composing the Ab-VDAD.

In the Ab-VDAD, the rate of comminution of particles with distance is likely to be a function of lithology and rock strength, as also observed in other studies (e.g., van Wyk De Vries et al., 2001; Clavero et al., 2002; Roverato et al., 2015). This process is particularly relevant to volcanic flank collapses as it is potentially intensified by the lower competence and potential hydrothermal alteration of material prior to failure (Thompson et al., 2009; van Wyk de Vries and Delcamp, 2015). This property constitutes the material easier to comminute and pulverise as suggested by Roverato et al. (2015) for the case of the Pungurehu VDA. Scoriaceous material appears to be the least competent encountered in the Ab-VDAD. Its cataclasis produces a diamicton composed of clasts in a fine interblock matrix, also described by Roverato et al. (2015). However, a similar cataclasis pattern is observed for all the lithologies in the Ab-VDAD to different degrees.

5.1.2 Fluidisation, spreading and stretching

At the outcrop scale, the most obvious feature of the deposit is the general stretching and thinning of lithological units in the EBF, which nonetheless preserve their lithological distinctness and stratigraphic sequence as illustrated in Figures 3, 4. The outline of the Ab-VDA blocks and their constituent lithological components becomes distorted by stretching as also described by Campbell et al. (1995) and Roberti et al. (2017), however, components maintain their relative position as they form bands in an arrangement of remnant stratigraphic sequence. Stretching and extension have been observed in other VDA/RA deposits (e.g., Siebert, 1984; Siebert et al., 1995; Schneider and Fisher, 1998; Clavero et al., 2002; Bernard et al., 2008; Shea et al., 2008; Roberti et al., 2017) after first described by Heim (1932) in the Elm RA (Switzerland). Stratigraphic sequence preservation has been observed for the Blackhawk RA (Shreve, 1968; Johnson, 1978) as well as VDADs (Ui and Glicken, 1986; Ui, 1989; Bernard et al., 2021) such as the Mount St. Helens (Glicken, 1991), and even for analogue (e.g., Hsü, 1975; Manzella and Labiouse, 2013) and numerical models (e.g., Campbell et al., 1995; Thompson et al., 2009).

Stretching of the EBF is interpreted to be a result of the laminar spreading of the mass during propagation. In a laminar flow regime, the spreading of granular material occurs parallel to the flow direction resulting in the stretching and thinning of units. Since particles are almost exclusively displaced parallel to the flow direction, lithological units preserve stratigraphic sequence. Sequence preservation suggests a spatially and temporally universal lack of large-scale turbulence and mixing in the Ab-VDA, as also suggested by other studies (Campbell et al., 1995; Reubi and Hernandez, 2000; Voight et al., 2002; Shea and van Wyk de Vries, 2008; Magnarini et al., 2021). Turbulence leads to chaotic distributions of flow direction and velocity within a fluid. The laminar fluidal behaviour is suggested to be the result of mechanical fluidisation of the material (Davies, 1982), as is also supported by the fluidal mixing of lithological units exhibited in Figures 3C, 4C. Also, the diffuse contacts suggest the fluid-like behaviour of clasts similar to agitated units in a fluid and gradual displacement and mixing due to agitation in a fluidised granular flow (van Wyk De Vries et al., 2001). The absence of fluid-escape or other interstitial fluid-related structures, sorting or laminated layers suggests a negligible initial and incorporated fluid content. Such features would have likely been at least partially preserved given the lack of turbulence and preservation continuity of stratigraphic sequences even at the most distal locations. Nonetheless, models of dry granular flows also generate fluidal contacts (Campbell et al., 1995; Thompson et al., 2009) like those observed in the Ab-VDAD and other deposits (e.g., Davies, 2015; van Wyk de Vries and Delcamp, 2015). However, the occurrence of stretched blocks throughout the height of the deposit is dissimilar to their occurrence only deeper near the base in other deposits such as the Chimborazo VDAD examined by Bernard et al. (2008). This observation suggests that stress, agitation and fluidisation of the mass were periodically distributed throughout the deposit and were not restricted to the base of the Ab-VDA.

5.1.3 Sedimentology and clast-size analysis

In VDAs/RAs, progressive fragmentation and comminution processes have been illustrated to produce a signal of gradual clast-size reduction with distance from the source (Bianchi Fasani, 2003; Crosta et al., 2007; Bustos et al., 2022) and gravel proportion decreasing as the proportion of sand-sized particles increases (Roverato et al., 2015; Makris et al., 2020).

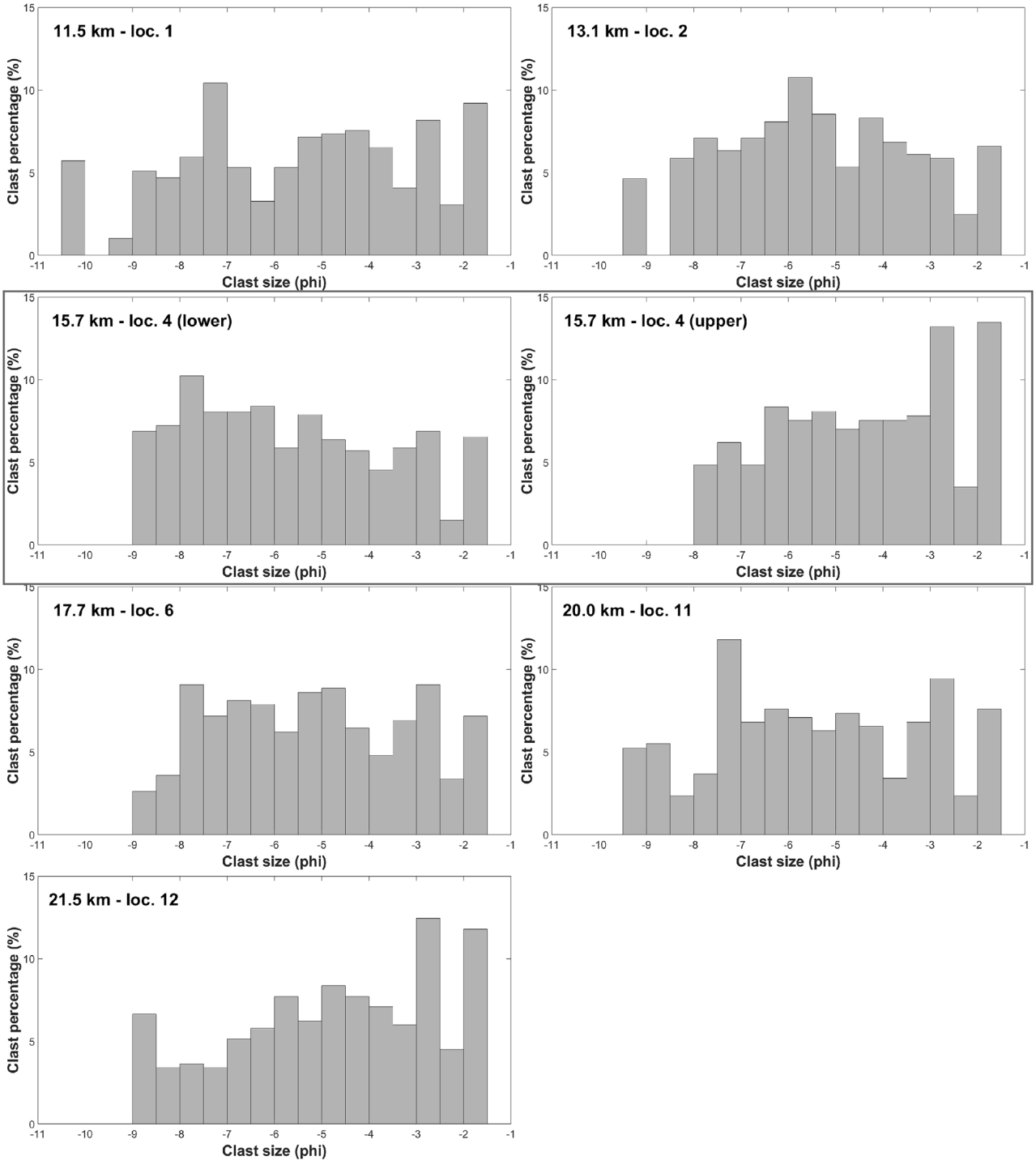

FIGURE 12
Clast-size distributions for clasts in the matrix-rich facies at different locations along the Abona volcanic debris avalanche deposit from proximal to distal.

Perinotto et al. (2015) also propose that the generation of finer material due to progressive comminution was responsible for the increased matrix with distance from the source that they observed. Therefore, an increase in the proportion of matrix compared to blocks with distance from the source would be expected in the Ab-VDAD. It would also be expected that the average clast size would be progressively reduced due to the gradual abrasion and fracturing of clasts in the agitated matrix (Schneider and Fisher, 1998; Perinotto et al., 2015; Paguican et al., 2021).

TABLE 1 Clast-size analysis at different locations along the Ab-VDAD. Location 4 is represented by 2 samples, one is from deeper closer to the base and one from shallower in the deposit, illustrated in Supplementary Appendix S3.

Loc./ sample	Distance from source (km)	90th percentile (mm)	75th percentile (mm)	50th percentile (mm)	25th percentile (mm)	10th percentile (mm)	Matrix proportion (%)
1	11.5	394.0	167.0	39.0	12.0	5.0	52.4
2	13.0	293.0	123.5	45.0	15.0	6.0	59.1
4 upper	15.7	321.0	167.0	61.5	16.0	6.0	54.7
4 lower	15.7	129.8	62.8	19.0	8.0	4.0	35.6
6	17.7	231.2	117.0	39.0	11.0	5.0	52.6
11	20.0	427.0	148.5	46.0	11.0	5.6	64.9
12	21.5	276.1	83.0	23.0	7.0	4.0	50.8

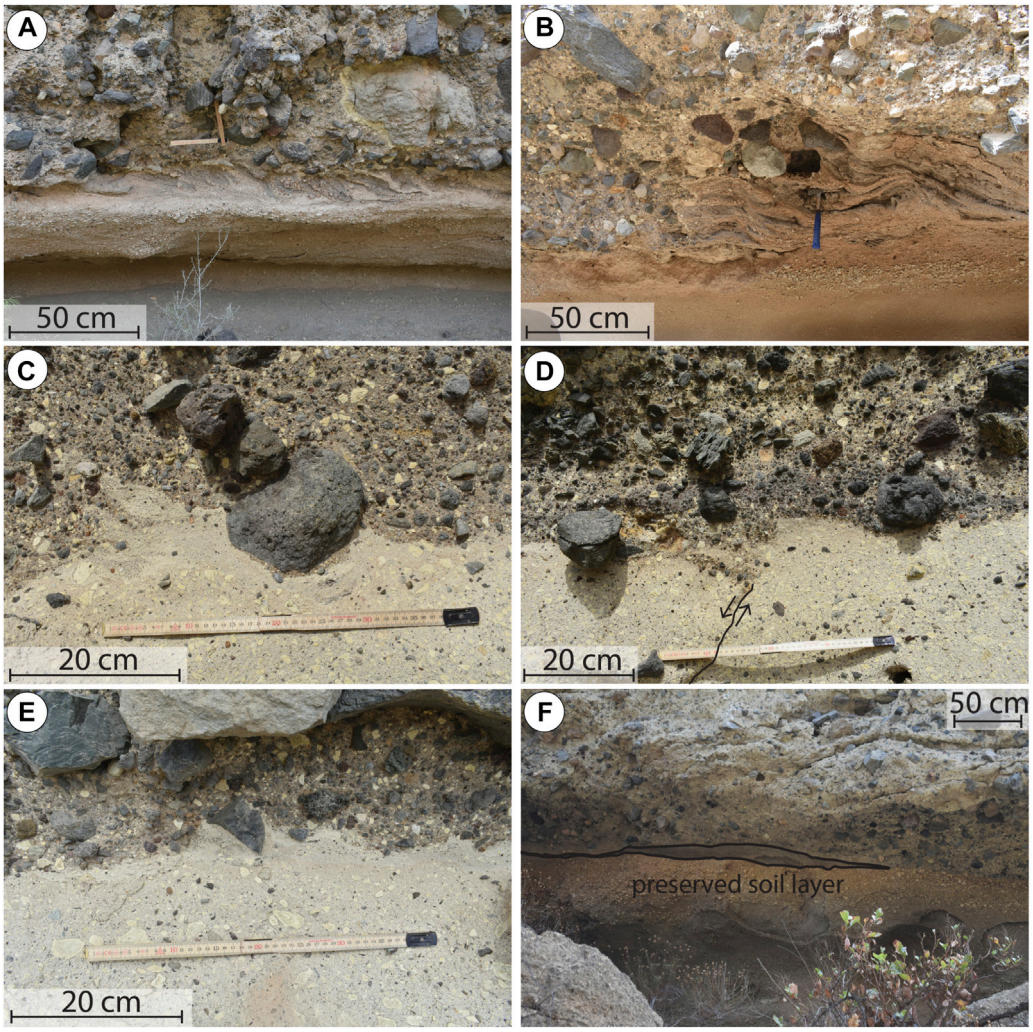

FIGURE 13
Interactions between the Abona volcanic debris avalanche deposit and the substrate. **(A)** Substrate bulldozing (location 10); **(B)** ploughing (location 7); **(C)** small-scale flame injection (location 12); **(D)** monolithological block in contact with the substrate, and faulting in the substrate due to the weight of the VDA (location 12); **(E)** the soil layer in the substrate is uneroded and almost unaffected by the passage of the avalanche at this segment (location 12); **(F)** the soil layer is locally preserved while eroded in adjacent segments of the contact (location 3).

Nonetheless, in the Ab-VDAD the proportion of matrix is highly variable in different locations both in the interblock and intrablock matrix and there is no systematic longitudinal evolution in the proportion of matrix and size of clasts composing the MF (Table 1). High variability has been observed within other VDA/RA deposits, but also between them (Hewitt et al., 2008). Likewise, the clast size percentiles in the MF of the Ab-VDAD do not exhibit a systematic longitudinal evolution (Figure 11; Table 1). Although a size reduction in the first 17.8 km can be inferred from the P90 and P75 percentiles evolution (Figure 11B), no consistent systematic correlation to the distance travelled is observed in data for the 10 km along which the deposit is exposed. A number of reasons are potentially responsible for the ambiguity of this signal:

1. The addition of material from the EBF to the MF interferes with the progressive fining of the clasts in the MF, which are the subject of the sampling. This addition of material is also not uniform, occurring at variable rates in the deposit. Although progressive cataclasis is likely to contribute to the content of fines in the MF with distance travelled, the distribution of the fining likely depends on the distribution of the stresses agitating the mass encouraging mixing and adding material from the EBF to the MF.
2. Since parts of the same block, with a different lithology exhibit different degrees of cataclasis (Figure 3D), the rate of comminution in blocks is not exclusively associated with the distance travelled. Instead, the degree of comminution is also a function of the lithology and the local stresses according to its location in the Ab-VDA. The lithological heterogeneity of the deposit results in an uneven distribution of comminution rate due to lithologies with different strength comminuting at different rates. Examining the Pungarehu and Cubilche VDADs, (Roverato et al., 2015; Roverato et al., 2018 respectively) observed that weaker lithologies, such as scoria, are more rapidly comminuted. This is in agreement with the observation of higher degrees of cataclasis in scoria compared to lavas in the Ab-VDAD (Figures 3D, 8). Scoriaceous material becomes cataclased to produce fine clasts in a fine intrablock matrix (Figure 8C). In contrast, lava lithologies produce coarser, more angular clasts and lower quantities of matrix (Figure 8B). This results in unsystematic interference in the relationship between comminution and the distance from the source.
3. Stress is not distributed uniformly in the deposit. This is the result of the uneven chaotic distribution of stress in ephemeral shear networks according to the instantaneous arrangement of the weight of the mass (as discussed in Section 5.3). Therefore, this enforces an unsystematic distribution of stress, and consequently comminution rate.

5.2 Substrate implications

The nature of the substrate deformation and erosion caused by a mass movement can offer information regarding its propagation dynamics (Dufresne et al., 2010b). Substrate folding, faulting and detachment features similar to those exhibited by the Ab-VDAD have been studied in various VDA/RA deposits (e.g., Schneider and Fisher, 1998; Belousov et al., 1999; van Wyk De Vries et al., 2001; Clavero et al., 2004; Bernard et al., 2008; Hewitt et al., 2008; Shea and van Wyk de Vries, 2008; Dufresne et al., 2010a), allowing evaluation through comparison of the propagation dynamics they represent. The pumice and pumice-rich ignimbrite substrate were mechanically weak, deformable and easy to erode during the propagation of the Ab-VDA. Detachment of the substrate into flame injections, substrate inclusions and the absence of the thin soil layer, as, for example, in Figure 13, suggests an erosional base locally. The substrate is mostly eroded by basal abrasion and ploughing. Basal abrasion is the process in which particles at the base slide parallel to particles in the substrate and mobilising them resulting in sharp erosional contacts (Gauer and Issler, 2004) like the one illustrated in Figure 7, in contrast to ploughing where the flow intrudes the substrate and pushes material out (Figures 13A, B). Impact erosion (e.g., Bernard et al., 2008; Dufresne, 2012) has potentially had a minor effect in the Ab-VDA, as illustrated by Figure 13C where the impact of a clast on the pumiceous topsoil layer is likely to have forced a flame injection.

Bulldozed, faulted, and ploughed substrate is evidence of local shear stresses between the Ab-VDA and the substrate. Below the Ab-VDAD this effect does not propagate deeper than 0.3–0.5 m (Figures 13B, D). This implies that due to the low coherence of the material, shear could not be effectively transmitted from the flow to the substrate. Compressional features, such as bulldozing and faulting, have been documented in other VDA/RA deposits with erodible substrate (e.g., Evans et al., 1994; Shea and van Wyk de Vries, 2008; Wang et al., 2019) as well as recreated in analogue experiments (Dufresne, 2012). The analogue experiments of Dufresne (2012) explore the relationship between a granular flow and different erodible substrate conditions using different granular materials to simulate diverse substrate properties. The findings support that low-friction material, like the pumice that constituted the substrate of the Ab-VDA, were readily mobilised and coupled with the granular mass. It is therefore likely that particles from the substrate under the Ab-VDA were easily detached through abrasion due to low cohesion, as demonstrated in Figure 7, which illustrates the incorporation of individual clasts from the substrate to the propagating mass. Small-scale flame injections similar to what is illustrated in the Ab-VDAD (Figure 13C) were also formed in the experiments where low friction material was briefly sheared between the avalanche and the substrate forming small clastic dikes before being incorporated. Therefore, the small scale of these features in the deposit also suggests a limited-strength substrate. The lack of large injections and scarcity blocks of the substrate in the Ab-VDAD reflects the low cohesion of the material that cannot be incorporated in one intact piece (Bernard et al., 2008). Incorporated components were quickly disaggregated as described by Hewitt et al. (2008) unlike other VDA/RA deposits where substrate blocks are preserved unmixed, like, for example, the Tschirgant RA (Dufresne et al., 2016b), the Nevado de Toluca VDAD (Caballero and Capra, 2011) and Cubilche VDAD (Roverato et al., 2018).

The substrate was locally bulldozed and eroded while in other areas remained undisturbed (e.g., Figure 13F). This unsystematic erosional pattern suggests a spatially variable accommodation of shear stress at the Ab-VDA base. In locations where high shear stress was accommodated at the base during the propagation, shear stress was transferred to the substrate, eroding or deforming it. However, where shear was accommodated in the body, the substrate remains intact. The lack of shear concentration at the base inhibited the degree of substrate perturbation. The uneven distribution of substrate perturbation

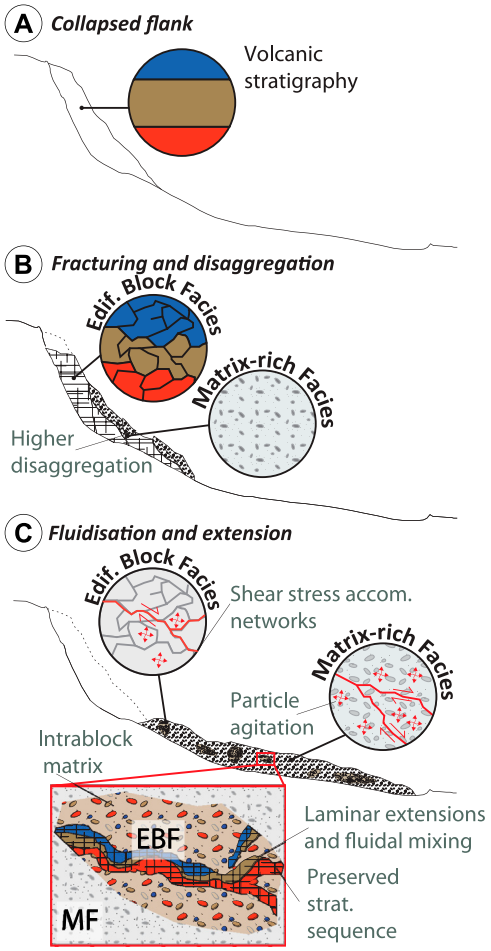

FIGURE 14
Schematic representation of the propagation and emplacement processes of the Abona debris avalanche. **(A)** Original stratigraphy prior to flank collapse. **(B)** Fracturing and disaggregation. The coarse fracturing leads to blocks with preserved stratigraphic sequences in the edifice block facies (EBF), whereas more intensely fractured areas evolve into the matrix-rich facies (MF). **(C)** Once the flank has disaggregated into a granular mass, ephemeral shear stress accommodation networks fluidise the material both in the MF and the EBF. Pockets of preserved stratigraphic sequence are preserved within the EBF where low degrees of stress and agitation have been accommodated (insert).

suggests that the Ab-VDA was not principally travelling as a plug with shear stress concentrated at the base, but as a fluidised granular mass where shear was distributed across the whole body of the flow.

5.3 Shear accommodation, propagation and emplacement model

VDAs result from flank collapses, propagating as slides immediately after the initial collapse and progressively evolving into granular flows (Voight et al., 1983; Siebert, 1984; Glicken, 1991; Scott et al., 2001). The behaviour of dry VDAs/RAs as dense granular flows with a partially collisional regime, where momentum transfer predominantly occurs through collisions, has been reinforced by several studies (e.g., Pierson and Costa, 1987; Iverson, 1997; Iverson and Denlinger, 2001; Dufresne and Davies, 2009; Roverato et al., 2015; Makris et al., 2020). Therefore, distinct element modelling (DEM) of individual interacting particles is suitable for investigating the dynamics of such granular flows, as supported by studies such as Cleary and Campbell (1993) and Crosta et al. (2001). The DEM simulations of Campbell et al. (1995) and Thompson et al. (2009) are of simplified granular flows with no bond between particles in the mass since their initiation. Particles are free to interact and are only affected by their collisions' momentum transfer, friction and potential energy transformed to kinetic. With these initial conditions, and no other external mechanisms, the collapsed masses evolve into granular flows. These simulations are successful in reproducing VDAD field observations of fluidal contacts, disperse boundaries and pockets of preserved stratigraphic sequence, like the ones observed in the Ab-VDAD. Characteristics of the simulated avalanches are also consistent with the laminar spreading and thinning of lithological units. Therefore, these models are suitable for the evaluation of propagation dynamics and processes of VDAs, which are characterised by a disaggregated and fragmented mass comparable to a granular flow as in the Ab-VDA. For this reason, their results are discussed in comparison with field observations in proposing a propagation model for the Ab-VDA.

The initial collapse of the Ab-VDA is likely to have been critical for the coarse fragmentation and disaggregation of the original mass (Figures 14A, B) due to the existence of an extensional regime (Longchamp et al., 2016), rapid unloading of lithostatic pressure (Belousov et al., 2007), and impact stresses (Voight et al., 1983; Glicken, 1991; Glicken, 1996; Bernard et al., 2008; Thompson et al., 2010). Areas that suffer the greatest strain and disaggregation at this stage are predisposed to evolve to the MF due to subsequent gradual homogenisation during propagation (Figure 14B) (Thompson et al., 2009; Roverato et al., 2015; Makris et al., 2023). According to Campbell et al. (1995), the preservation of jigsaw-fractured blocks reflects local minimal agitation during propagation. The scarcity of jigsaw-fractured blocks in the Ab-VDAD supports that the disaggregation was not a process that occurred by the impulsive stress of the initial collapse, or during a violent termination of the mass. In lack of agitation except in specific impulses fractures would have been preserved in undisaggregared material (Campbell et al., 1995; Reubi and Hernandez, 2000; Clavero et al., 2002; Thompson et al., 2010). Instead, the diamicton texture of the Ab-VDA EBF suggests that the entirety of the mass periodically experienced strain and agitation during propagation (Figure 14C).

Further fragmentation and disaggregation transform the material into a granular mass where independent particles could engage in collisions (Ogawa, 1978; Campbell, 1990; Iverson, 1997; Roche et al., 2006). The elimination of particles greater than −9.5φ and reduction of the P90 and P75 percentile clast sizes in the first 17.6 km of the Ab-VDA (Figures 11, 12) are likely to be a signal of the fracturing and comminution. Once the mass fractures, disaggregates and becomes granular a VDA can behave as a granular flow and assume fluidal behaviour at least locally (Figure 14C) (Voight et al., 1983; Glicken, 1996; Schneider and Fisher, 1998; Hewitt et al., 2008; Makris et al., 2020). Fluidal contacts between lithological units (Figures 3A, C, 4B, C) and diffuse boundaries (Figure 10) suggest that the material constituted a

granular fluidised mass enabled by the agitation/vibration and collisions of independently interacting particles generating a granular temperature (Ogawa, 1978; Campbell, 1990; Iverson, 1997; Armanini et al., 2005; Roche et al., 2006). The process was likely enhanced in the Ab-VDA by the abundance of less competent lithologies like scoria and pumice, which require little energy to fracture and evolve into a granular material. Granular temperature measures the random vibration of particles and the agitation in the mass (Brilliantov and Pöschel, 2010). The concept of granular temperature is vital for understanding the behaviour of rapid granular flows as highlighted by Campbell (1990). As the agitation in a granular material increases and particle collisions are more frequent, relative to frictional contacts, the material dilates and behaves similarly to a fluid (Campbell, 1990; Brilliantov and Pöschel, 2010; Johnson et al., 2016). This behaviour is achieved by the transition from a quasistatic frictional regime, with predominantly persistent frictional contacts, to a rapid granular flow collisional regime (Drake, 1991; Campbell, 2005). In a collisional regime, particles are frequently engaged in collisions, to the extent that the mass approaches the behaviour of a molecular gas or fluid (Johnson et al., 2016). The transition to the fluidised behaviour, illustrated in Figure 14C, results in the reduction of effective friction due to the propagation achieved by particles when they are momentarily relieved of the static burden of the overlying weight after a collision, in the time they are not involved in frictional contacts (Melosh, 1979). The mixing which resulted in the homogenous MF and the incompletely mixed intrablock matrix in Ab-VDA is not the result of turbulence, but rather gradual homogenisation due to the agitation and diffusion of granular particles (Perinotto et al., 2015; Roverato et al., 2015) as visualised in Figure 10, and explained in Makris et al. (2023). Gradual homogenisation is the result of agitated particles vibrating and gradually displacing and chaotically mixing. Diffuse boundaries due to the agitation, vibration and displacement of the particles lead to the diffusion of units away from the boundary, and particles from the matrix filling the gaps. This behaviour is best demonstrated by the diffuse boundaries in Figure 10. The mixing eventually results in a homogenous unit such as the intrablock matrix illustrated in Figure 3C, and from the interblock matrix in Figure 6A.

The lack of faults and brittle deformation in the deposit supports a fluidised Ab-VDA with no sections that sustained adequate coherence for brittle behaviour. Similarly, the universal microfracturing and fluidal features in the Ab-VDAD support that stresses were distributed throughout the mass (Pollet and Schneider, 2004; Friedmann et al., 2006; Dufresne et al., 2016a; Wang et al., 2019), and were not concentrated in long-lived shear zones either at the base or in the body of the flow (Figure 14). Nonetheless, the observation of preserved stratigraphic sequences and stretched continuous lithological units demonstrate that the emplacement remained laminar, without turbulence as also suggested in the DEM simulations of Thompson et al. (2010). The fluid-like behaviour combined with the laminar spreading produced the lenticular stretched shape and fluidal features in the EBF (e.g., Figure 3). However, it is unlikely that VDAs are pure rapid granular flows with an exclusively collisional regime (Campbell et al., 1995; Johnson et al., 2016). It is more probable that particles in the Ab-VDA were engaged in frictional contacts for the majority of the propagation, thus adopting a behaviour between a rapid and quasistatic granular flow regime. Shear was accommodated in chaotically distributed, ephemeral energy chains, as distributed in Figure 14C, constituting temporary shear networks as described by Davies and McSaveney (2009), Thompson et al. (2009) and Dufresne et al. (2016a). Such shear zones are not necessarily continuously or constantly active during propagation. These energy chains form according to the instantaneous distribution of the self-weight of the material and are dissimilar to the uniform distribution in liquids or homogenous solids (De Blasio, 2011). Therefore, intergranular stresses are temporarily concentrated in these short-lived, interlinked assemblages aligned to the shear direction (Sammis et al., 1987; Anthony and Marone, 2005; Mair and Hazzard, 2007; Sammis and King, 2007; Furbish et al., 2008). In such a deforming granular medium, grain bridges are continuously forming and breaking, producing highly heterogeneous deposits (Hooke and Iverson, 1995), as observed in the Ab-VDAD. Consequently, stress accommodation and granular behaviour were likely temporally and spatially variable in different sections of the Ab-VDA. Stress distribution heterogeneity within the propagating material is also suggested by Magnarini et al. (2021) through their study of the El Magnifico RA deposit (Atacama, Chile). This heterogeneity is also evident in the quantitative clast-size analysis, which reveals an unsystematic clast-size distribution variation with propagation distance. Moreover, the ephemeral and unsystematic distribution of the shear accommodation is evident from the spatially variable substrate perturbation, discussed in Section 5.2. The ephemeral nature means that shear leaves no detectable trace in the sedimentological record as short-lived shear networks rearrange to different configurations through the deposit (Davies and McSaveney, 2009). Indeed, in the Ab-VDAD no zones of concentrated shear with distinct sedimentology are exhibited in the deposit, either at the base or within its body. Ephemeral shear accommodation in slip microsurfaces distributed throughout the mass and the base result in the cataclasis, disaggregation of the mass and the creation of the interblock and intrablock matrix. Internal shear accommodation (as opposed to basal) is more common in VDAs than they are in RAs (Dunning, 2004; Crosta et al., 2007; Davies and McSaveney, 2009). Roverato et al. (2015) suggest that the easier pulverisation of weak volcanic material, like scorias, is likely to encourage the formation of a fine matrix capable of accommodating shear. It is therefore likely that the source of the Ab-VDAD was a flank composed of weak material which was potentially already fractured or hydrothermally altered or weathered (Glicken, 1991; Palmer et al., 1991; Belousov et al., 1999; Bernard et al., 2008; Shea et al., 2008; Roverato et al., 2015). Therefore, the Ab-VDA has suffered more widespread disaggregation compared to VDAs/RAs composed of more competent material, such as the Tenteniguada VDAD (Makris et al., 2023). In the Thompson et al. (2009) model the unsystematic distribution of stresses leads to pockets of material remaining less disaggregated, where less stress has been accommodated. Pockets of EBF preserved stratigraphic sequence in the Ab-VDAD, as illustrated in Figure 4, represent areas that happened not to experience high stresses during propagation. The properties exhibited by the Ab-VDAD offer field evidence to support these processes, which have so far only been proposed theoretically.

The DEM simulations mentioned reproduce a process in which a purely gravity-driven homogenous avalanche can evolve into a flow due to increasing momentum and kinetic energy from its initial potential energy (Thompson et al., 2009). The sedimentological features of the AB-VDA are in agreement with the process of

collective motion, distributed stresses and spreading in a laminar manner that the granular flow produces in Thompson et al. (2009). The findings support that the Ab-VDA was purely gravitational with no additional auxiliary friction-reducing mechanisms. The initial coherent sliding mass evolved into a flow with distributed shear stress generating *in situ* fragmentation, as described in the VDADs examined by Reubi and Hernandez (2000). The syn-propagation fracturing and disaggregation of the mass were driven by the kinetic energy from the initial acceleration resulting in interparticle collisions as in the process described by Perinotto et al. (2015).

5.4 Implications for volcanic debris avalanche long runout and mobility mechanisms

Paguican et al. (2021) propose three potential flow regime models for the runout dynamics of VDAs. 1) The plug flow model involves a coherent, poorly disaggregated mass transported over a highly deformed low friction shear layer at the base (Voight et al., 1983; Takarada et al., 1999). 2) In the transitional slide model spreading of the mass is accommodated in listric normal faults merging in a basal sliding plane (van Wyk De Vries et al., 2001; Paguican, 2012). The observations presented here suggest that the Ab-VDA is not compatible with the models of plug flow and translational slide due to the lack of a basal shear layer, and listric faults respectively. The presented findings add to the evidence that a low frictional basal layer is not the universal explanation for the mobility of long runout VDAs/RAs (Johnson et al., 2016). The third, 3) multiple shear zone model (Paguican et al., 2021) proposes the existence of zones of shear accommodation hosted by a matrix created by weaker lithologies within the body of a flow. These zones form a network around, harder, difficult-to-fracture lithologies, effectively sheltering them from shear stress (Roverato et al., 2015). This is not observed in this deposit either, potentially due to the lack of a significant amount of competent material. Therefore, a new alternative shear accommodation variation of the third model is here proposed for the Ab-VDA, where shear is distributed throughout the fractured granular mass, as also suggested by Campbell et al. (1995) for loose granular material. The proposed model is of a partially fluidised granular flow with distributed shear in temporary shear networks.

Since the 1960s hypotheses and models have been proposed regarding the enhanced mobility of VDAs/RAs based on morphology, internal architecture, sedimentology, theoretical approaches, and numerical and analogue models (reviewed in Davies, 1982; Erismann and Abele, 2001; Hungr, 2002; Legros, 2002; Collins and Melosh, 2003; Friedmann et al., 2006; Manzella and Labiouse, 2008; Davies and McSaveney, 2012). Among those, for the Ab-VDA Dávila-Harris et al. (2011) suggest that the progressive fragmentation of the mass is most consistent with the acoustic fluidisation mechanism proposed by Melosh (1979), with shock waves propagating through the solid moving mass. According to Melosh (2015), vibrations create transient, high-frequency pressure fluctuations (or acoustic waves) in the propagating mass, that fluidise the homogenous debris through local variations in contact forces. These pressure fluctuations instantaneously relieve the overburden weight on individual clasts that become free to slip. This process creates an agitated laminar flow with low mixing between units and is capable of enhancing the mobility of granular flows (Collins and Melosh, 2003). The numerical modelling of Collins and Melosh (2003) suggests that under high-frequency pressure vibrations, a granular mass will develop into a fluid-like flow with uniform viscosity. The observations from the Ab-VDAD are in agreement with the velocity profiles reproduced by the DEM simulations of Campbell et al. (1995) and Johnson et al. (2016) and the processes and sedimentology generated are compatible with the acoustic fluidisation hypothesis (Johnson et al., 2016). Acoustic fluidisation could be the source of the distributed shear in an agitated mass with collisional contacts between particles generating a fluid-like behaviour in a flow that remains laminar. The simulations of Campbell et al. (1995) even reproduce the stratigraphic preservation, despite the bulk fluidisation of the flow, as also observed in the Ab-VDAD. This is the result of the uneven distribution of stress implied by the acoustic fluidisation mechanism (Melosh, 1979; Magnarini et al., 2021).

On the other hand, dynamic fragmentation is another process potentially active during the propagation of the Ab-VDA. Dynamic fragmentation is the effect generated by the fracturing of intact rock under rapid strain and confining pressure and can preserve the dilated state in a granular material as supported by studies such as Davies et al. (2010) and Zhang and McSaveney (2017). Prior to fracturing, particles deform plastically under the shearing motion around them. When these forces exceed the local strength of a particle, it breaks and generates fractures. A proportion of the stored elastic energy is then released with the fractures radiating from the centre of mass of the clast. The elastic energy released during disintegration could contribute to the enhanced mobility of VDAs/RAs. This theory is disputed by Rait and Bowman (2016) with shear tests suggesting that kinetic energy produced in this manner is quickly dissipated in the matrix with no long-lasting impact. Nonetheless, Paguican et al. (2021) suggest that elastic energy in combination with acoustic fluidisation waves might be responsible for fracturing and dilatancy of a granular mass. Whether elastic energy or acoustic waves enhanced the mobility of the material cannot be confirmed by the findings of this study, but both these theories are consistent with the field observations of the Ab-VDA. Both mechanisms do not require the presence of exotic processes, which confirms the ability of VDA to show high mobility by internally generated mechanisms.

6 Conclusion

The distribution of facies and structures and sedimentological analysis, in comparison with conceptual and numerical models and other VDA/RA deposits, have led to the following conceptual model for the propagation dynamics of the Ab-VDA:

1. The source mass was composed mainly of pyroclastic material and a small proportion of lavas (Figure 14A). Due to the high cataclasis of the material it is assumed possible that the material could have been hydrothermally altered or weathered, weakened and preconditioned for fracturing. The destabilisation and collapse of the mass occurred during an explosive eruption.
2. The initial slide phase led to a coarse disaggregation of the mass and generated fractures, splitting the mass into blocks that

preserved their internal sedimentary sequence. Areas that sustained more strain were more intensely fractured and later disaggregated and evolved into the MF through gradual homogenisation (Figure 14B).

3. Once the mass moved out of the failure scarp it evolved into a flow and experienced laminar spreading. This is likely because the front of the flow was travelling faster than the proximal part, leading to the extension and elongation of the mass, including embedded blocks. This was enabled by the high degree of microfracturing of the material constituting the mass granular, with particles capable of moving independently and engaging in collisions (Figure 14C). Collisional/vibrational contacts between particles in the mass gradually led to the microfractured diamicton texture of the block facies through both disaggregation of existing fractures and comminution due to grain interactions. The agitation gave the mass a granular temperature causing it to behave as a fluidised granular mass. This led to the fluidal features and diffuse contacts observed in the deposit. Mixing within the blocks was minimal, caused by gradual homogenisation. This behaviour was enabled due to the weakness of the material and the resultant disaggregation that allowed spatially distributed shear instead of concentrated shear at the base or in shear zones.
4. The shear stress of this movement was distributed unsystematically in ephemeral networks throughout the body and the base of the mass. The spatially and temporally variable nature of the shear accommodation is also reflected in the inconsistent influence of the flow on the substrate. Areas where shear was high exhibit bulldozing and substrate incorporation while in areas of low shear the substrate remains unaffected. The low coherence of the substrate is evident by the disaggregation of incorporated material and the shallow deformation beneath the flow that did not allow shear to be transmitted deep underneath the Ab-VDA.
5. The unsystematic distribution of stresses and therefore mixing and comminution in the mass is responsible for the lack of a longitudinal evolution in the clast size and the proportion of matrix illustrated in the deposit through the quantitative clast-size and matrix-content analysis of the MF.
6. The result of these processes is the emplacement of a microfractured deposit with pockets of EBF and preserved stratigraphy surrounded by the MF (Figure 14C).

The present findings add to the evidence that challenges the view that all long runout VDAs/RAs propagate as a plug on a low frictional basal layer accommodating the shear of the propagating mass (Campbell et al., 1995; Johnson et al., 2016). They add to the body of recent evidence that the shear is distributed randomly in ephemeral networks throughout the avalanche as well as the base (Davies and McSaveney, 2009; Dufresne et al., 2016a). The observations are also compatible with both the theories of acoustic fluidisation and dynamic fragmentation that could have been active during the propagation of the mass.

This study highlights the importance of field studies for understanding VDA propagation dynamics. The novel methodology for the sedimentological examination of indurated deposits presented here provides a new tool to study deposits that were not considered before, increasing the capacity for collecting field evidence and to further understand VDA/RAs and the hazard they pose.

Data availability statement

The original contributions presented in the study are included in the article/Supplementary Material, further inquiries can be directed to the corresponding author.

Author contributions

SM: Conceptualization, investigation, methodology, writing—original draft, visualization; MR: Conceptualization, investigation, writing- reviewing and editing; PD-H: Investigation, visualization, writing- reviewing and editing; PC: Conceptualization, investigation, writing- reviewing and editing; IM: Conceptualization, investigation, writing- reviewing and editing, supervision. All authors listed have made a substantial, direct, and intellectual contribution to the work and approved it for publication.

Funding

The fieldwork for this study was funded by the Geological Society of London through a Research Grant. The publishing costs were covered by funding allocated from the University of Plymouth Frontiers Open Access publishing external funding.

Conflict of interest

The authors declare that the research was conducted in the absence of any commercial or financial relationships that could be construed as a potential conflict of interest.

Publisher's note

Supplementary material

The Supplementary Material for this article can be found online at: https://www.frontiersin.org/articles/10.3389/feart.2023.1177507/full#supplementary-material

References

Alloway, B., Mc Comb, P., Neall, V., Vucetich, C., Gibb, J., Sherburn, S., et al. (2005). Stratigraphy, age, and correlation of voluminous debris-avalanche events from an ancestral Egmont Volcano: Implications for coastal plain construction and regional hazard assessment. *J. R. Soc. New Zeal.* 35, 229–267. doi:10.1080/03014223.2005.9517782

Anthony, J. L., and Marone, C. (2005). Influence of particle characteristics on granular friction. *J. Geophys. Res. Solid Earth* 110, B08409. doi:10.1029/2004jb003399

Armanini, A., Capart, H., Fraccarollo, L., and Larcher, M. (2005). Rheological stratification in experimental free-surface flows of granular-liquid mixtures. *J. Fluid Mech.* 532, 269–319. doi:10.1017/S0022112005004283

Attal, M., and Lavé, J. (2006). Changes of bedload characteristics along the Marsyandi River (central Nepal): Implications for understanding hillslope sediment supply, sediment load evolution along fluvial networks, and denudation in active orogenic belts. *Spec. Pap. Geol. Soc. Am.* 398, 143–171. doi:10.1130/2006.2398(09

Banton, J., Villard, P., Jongmans, D., and Scavia, C. (2009). Two-dimensional discrete element models of debris avalanches: Parameterization and the reproducibility of experimental results. *J. Geophys. Res. Earth Surf.* 114, F04013–F04015. doi:10.1029/2008JF001161

Bates, R. L., and Jackson, J. A. (1984). *Dictionary of geological terms*. New York City: Anchor Books.

Belousov, A., Belousova, M., and Voight, B. (1999). Multiple edifice failures, debris avalanches and associated eruptions in the Holocene history of Shiveluch volcano, Kamchatka, Russia. *Bull. Volcanol.* 61, 324–342. doi:10.1007/s004450050300

Belousov, A., Voight, B., and Belousova, M. (2007). Directed blasts and blast-generated pyroclastic density currents: A comparison of the bezymianny 1956, Mount St helens 1980, and soufrière hills, Montserrat 1997 eruptions and deposits. *Bull. Volcanol.* 69, 701–740. doi:10.1007/s00445-006-0109-y

Berends, S. H., (2018). Grain size analysis by thin section images of Permian deep-marine sediments from the Fort Brown Formation, Karoo Basin, South Africa (Master's thesis).

Bernard, B., Takarada, S., Andrade, S. D., and Dufresne, A. (2021). "Terminology and strategy to describe large volcanic landslides and debris avalanches," in *Volcanic debris avalanches: From collapse to hazard*. Editors M. Roverato, A. Dufresne, and J. Procter (Heidelberg, Germany: Springer book series advances in volcanology), 51–73.

Bernard, B., van Wyk de Vries, B., Barba, D., Leyrit, H., Robin, C., Alcaraz, S., et al. (2008). The Chimborazo sector collapse and debris avalanche: Deposit characteristics as evidence of emplacement mechanisms. *J. Volcanol. Geotherm. Res.* 176, 36–43. doi:10.1016/j.jvolgeores.2008.03.012

Bernard, K., Thouret, J. C., and van Wyk de Vries, B. (2017). Emplacement and transformations of volcanic debris avalanches-A case study at El Misti volcano, Peru. *J. Volcanol. Geotherm. Res.* 340, 68–91. doi:10.1016/j.jvolgeores.2017.04.009

Bernard, K., and van Wyk de Vries, B. (2017). Volcanic avalanche fault zone with pseudotachylite and gouge in French Massif Central. *J. Volcanol. Geotherm. Res.* 347, 112–135. doi:10.1016/j.jvolgeores.2017.09.006

Bianchi Fasani, G., (2003). Grandi Frane in roccia: fenomenologia ed evidenze di terreno, Tesi di Dottorato: Università degli Studi di Roma "La Sapienza"

Blair, T. C., and McPherson, J. G. (1999). Grain-size and textural classification of coarse sedimentary particles. *J. Sediment. Res.* 69, 6–19. doi:10.2110/jsr.69.6

Blair, T. C. (1987). Sedimentary processes, vertical stratification sequences, and geomorphology of the Roaring River alluvial fan, Rocky Mountain National Park, Colorado. *J. Sediment. Pet.* 57, 1–18. doi:10.1306/212F8A8A-2B24-11D7-8648000102C1865D

Brilliantov, N. V., and Pöschel, T. (2010). *Kinetic theory of granular gases*. Oxford, UK: Oxford University Press on Demand.

Bryan, S. E., Martí, J., and Cas, R. A. F. (1998). Stratigraphy of the Bandas del Sur Formation: an extracaldera record of Quaternary phonolitic explosive eruptions from the Las Cañadas edifice, Tenerife (Canary Islands). *Geol. Mag.* 135, 605–636. doi:10.1017/s0016756897001258

Bunte, K., and Abt, S. R. (2001). *Sampling surface and Subsurface particle-size distributions in wadable gravel- and cobble-bed Streams for analyses in sediment transport, Hydraulics, and streambed monitoring*. Washington, DC: US Dep. Agric. For. Serv. Rocky Mt. Res. Station., 450.

Buscombe, D. (2008). Estimation of grain-size distributions and associated parameters from digital images of sediment. *Sediment. Geol.* 210, 1–10. doi:10.1016/j.sedgeo.2008.06.007

Bustos, E., Capra, L., and Norini, G. (2022). Volcanic debris avalanche transport and emplacement at Chimpa volcano (Central Puna, Argentina): Insights from morphology, grain-size and clast surficial textures. *J. Volcanol. Geotherm. Res.* 432, 107671. doi:10.1016/j.jvolgeores.2022.107671

Caballero, L., and Capra, L. (2011). Textural analysis of particles from El Zaguán debris avalanche deposit, Nevado de Toluca volcano, Mexico: Evidence of flow behavior during emplacement. *J. Volcanol. Geotherm. Res.* 200, 75–82. doi:10.1016/j.jvolgeores.2010.12.003

Campbell, C. S., Cleary, P. W., and Hopkins, M. (1995). Large-scale landslide simulations: Global deformation, velocities and basal friction. *J. Geophys. Res.* 100, 8267–8283. doi:10.1029/94JB00937

Campbell, C. S. (1990). Rapid granular flows. *Annu. Rev. Fluid Mech.* 22, 57–90. doi:10.1146/annurev.fl.22.010190.000421

Campbell, C. S. (2005). Stress-controlled elastic granular shear flows. *J. Fluid Mech.* 539, 273–297. doi:10.1017/s0022112005005616

Cas, R. A. F., Wolff, J. A., Martí, J., Olin, P. H., Edgar, C. J., Pittari, A., et al. (2022). Tenerife, a complex end member of basaltic oceanic island volcanoes, with explosive polygenetic phonolitic calderas, and phonolitic-basaltic stratovolcanoes. *Earth-Science Rev.* 230, 103990. doi:10.1016/j.earscirev.2022.103990

Casagli, N., Ermini, L., and Rosati, G. (2003). Determining grain size distribution of the material composing landslide dams in the Northern Apennines: Sampling and processing methods. *Eng. Geol.* 69, 83–97. doi:10.1016/S0013-7952(02)00249-1

Chayes, F. (1956). *Petrographic modal analysis*. New York: John Wiley.

Clavero, J., Polanco, E., Godoy, E., Aguilar, G., Sparks, R. S. J., de Vries, B. V. W., et al. (2004). Substrata Influence in the transport and emplacement mechanism of the Ollagüe Debris Avalanche (Northern Chile). *Acta Vulcanologica* 16 (1-2), 59–76.

Clavero, J., Sparks, R., Huppert, H., and Dade, W. (2002). Geological constraints on the emplacement mechanism of the Parinacota debris avalanche, Northern Chile. *Bull. Volcanol.* 64, 40–54. doi:10.1007/s00445-001-0183-0

Cleary, P. W., and Campbell, C. S. (1993). Self-lubrication for long runout landslides: Examination by computer simulation. *J. Geophys. Res. Solid Earth* 98, 21911–21924. doi:10.1029/93jb02380

Collins, G. S., and Melosh, H. J. (2003). Acoustic fluidization and the extraordinary mobility of sturzstroms. *J. Geophys. Res. Solid Earth* 108, 1–14. doi:10.1029/2003jb002465

Crosta, G. B., Calvetti, F., Imposimato, S., Roddeman, D., Frattini, P., and Agliardi, F. (2001). Granular flows and numerical modelling of landslides. *Rep. DAMOCLES Proj.* 2001, 16–36.

Crosta, G. B., Frattini, P., and Fusi, N. (2007). Fragmentation in the val Pola rock avalanche, Italian Alps. *J. Geophys. Res. Earth Surf.* 112, F01006–F01023. doi:10.1029/2005JF000455

Cruden, D. M., and Varnes, D. J. (1996). "Landslide types and processes," in *Landslides-investigation and mitigation*. Editors A. .K. Turner and R. .L. Schuster (Washington DC: National Academy Press), 36–75.

Cuomo, S. (2020). Modelling of flowslides and debris avalanches in natural and engineered slopes: A review. *Geoenvironmental Disasters* 7, 1–25. doi:10.1186/s40677-019-0133-9

Davies, T., (2015). Landslide hazards, risks, and disasters: introduction. *In Landslide Hazards, Risks, and Disasters*. Academic Press, 1–16.

Davies, T., and McSaveney, M. J. (1999). Runout of dry granular avalanches. *Can. Geotech. J.* 36, 313–320. doi:10.1139/t98-108

Davies, T., and McSaveney, M. J. (2009). The role of rock fragmentation in the motion of large landslides. *Eng. Geol.* 109, 67–79. doi:10.1016/j.enggeo.2008.11.004

Davies, T., McSaveney, M., and Kelfoun, K. (2010). Runout of the Socompa volcanic debris avalanche, Chile: A mechanical explanation for low basal shear resistance. *Bull. Volcanol.* 72, 933–944. doi:10.1007/s00445-010-0372-9

Davies, T., and McSaveney, M. (2012). "Mobility of long-runout rock avalanches," in *Landslides–types, mech. Model.* Editors J. .J. Clague and D. Stead (Cambridge: Cambridge University Press), 50–58.

Davies, T. (1982). Spreading of rock avalanche debris by mechanical fluidization. *Rock Mech.* 24, 9–24. doi:10.1007/bf01239474

Dávila-Harris, P., Branney, M. J., and Storey, M. (2011). Large eruption-triggered ocean-island landslide at Tenerife: Onshore record and long-term effects on hazardous pyroclastic dispersal. *Geology* 39, 951–954. doi:10.1130/G31994.1

Dávila-Harris, P., Branney, M. J., Storey, M., Taylor, R. N., and Sliwinski, J. T. (2023). The upper Pleistocene (1.8-0.7 Ma) explosive eruptive history of Las Cañadas, ocean-island volcano, Tenerife. *J. Volcanol. Geotherm. Res.* 436, 107777. doi:10.1016/j.jvolgeores.2023.107777

De Blasio, F. V. (2011). *Introduction to the physics of landslides*. Heidelberg, Germany: Springer book series advances in volcanology. doi:10.1007/978-94-007-1122-8

Detert, M., Weitbrecht, V., et al. (2020). "Determining image-based grain size distribution with suboptimal conditioned photos," in *River Flow 2020*. Editors W. Uijttewaal, M. J. Franca, D. Valero, V. Chavarrias, C. Ylla Arbos, and R. Shielen (Lodon: CRC Press), 1045–1052.

Di Traglia, F., Bartolini, S., Artesi, E., Nolesini, T., Ciampalini, A., Lagomarsino, D., et al. (2018). Susceptibility of intrusion-related landslides at volcanic islands: The stromboli case study. *Landslides* 15, 21–29. doi:10.1007/s10346-017-0866-z

Drake, T. G. (1991). Granular flow physical experiments and their implications for microstructural theories. *J. Fluid Mech.* 225, 121–152. doi:10.1017/S0022112091001994

Dufresne, A., Bösmeier, A., and Prager, C. (2016a). Sedimentology of rock avalanche deposits – case study and review. *Earth-Science Rev.* 163, 234–259. doi:10.1016/j.earscirev.2016.10.002

Dufresne, A., and Davies, T. (2009). Longitudinal ridges in mass movement deposits. *Geomorphology* 105, 171–181. doi:10.1016/j.geomorph.2008.09.009

Dufresne, A., Davies, T., and McSaveney, M. J. (2010a). Influence of runout-path material on emplacement of the Round Top rock avalanche, New Zealand. *Earth Surf. Process. Landforms* 35, 190–201. doi:10.1002/esp.1900

Dufresne, A., and Dunning, S. (2017). Process dependence of grain size distributions in rock avalanche deposits. *Landslides* 14, 1555–1563. doi:10.1007/s10346-017-0806-y

Dufresne, A. (2012). Granular flow experiments on the interaction with stationary runout path materials and comparison to rock avalanche events. *Earth Surf. Process. Landforms* 37, 1527–1541. doi:10.1002/esp.3296

Dufresne, A., Prager, C., and Bösmeier, A. (2016b). Insights into rock avalanche emplacement processes from detailed morpho-lithological studies of the Tschirgant deposit (Tyrol, Austria). *Earth Surf. Process. Landforms* 41, 587–602. doi:10.1002/esp.3847

Dufresne, A., Salinas, S., and Siebe, C. (2010b). Substrate deformation associated with the Jocotitlán edifice collapse and debris avalanche deposit, Central México. *J. Volcanol. Geotherm. Res.* 197, 133–148. doi:10.1016/j.jvolgeores.2010.02.019

Dunning, S. (2004). *Rock avalanches in high mountains*. PhD Thesis.

Erismann, T. H., and Abele, G. (2001). *Dynamics of rockslides and rockfalls*. Heidelberg, Germany: Springer Science & Business Media. doi:10.1017/CBO9781107415324.004

Erismann, T. H. (1979). Mechanisms of large landslides. *Rock Mech. Felsmech. Mécanique Des. Roches* 12, 15–46. doi:10.1007/BF01241087

Evans, S., Hungr, O., and Enegren, E. G. (1994). The avalanche lake rock avalanche, mackenzie mountains, northwest territories, Canada: Description, dating, and dynamics. *Can. Geotech. J.* 31, 749–768. doi:10.1139/t94-086

Ferraro, F., Grieco, D. S., Agosta, F., and Prosser, G. (2018). Space-time evolution of cataclasis in carbonate fault zones. *J. Struct. Geol.* 110, 45–64. doi:10.1016/j.jsg.2018.02.007

Friedmann, S. J., Taberlet, N., and Losert, W. (2006). Rock-avalanche dynamics: Insights from granular physics experiments. *Int. J. Earth Sci.* 95, 911–919. doi:10.1007/s00531-006-0067-9

Furbish, D. J., Schmeekle, M. W., and Roering, J. J. (2008). Thermal and force-chain effects in an experimental, sloping granular shear flow. *Earth Surf. Process. Landforms* 33, 2108–2117. doi:10.1002/esp.1655

Gauer, P., and Issler, D. (2004). Possible erosion mechanisms in snow avalanches. *Ann. Glaciol.* 38, 384–392. doi:10.3189/172756404781815068

Glicken, H. (1996). *Rockslide-debris avalanche of may 18, 1980*. Washington: USGS Open File Report.

Glicken, H. (1991). Sedimentary architecture of large volcanic-debris avalanches. *Sediment. Volcan. Settings* 1991, 99–106. doi:10.2110/pec.91.45.0099

Harvey, E. L., Hales, T. C., Hobley, D. E. J., Liu, J., and Fan, X. (2022). Measuring the grain-size distributions of mass movement deposits. *Earth Surf. Process. Landforms* 47, 1599–1614. doi:10.1002/esp.5337

Heim, A. (1932). *Bergsturz und menschenleben*. Fretz & Wasmuth 77.

Hewitt, K., Clague, J. J., and Orwin, J. F. (2008). Legacies of catastrophic rock slope failures in mountain landscapes. *Earth-Science Rev.* 87, 1–38. doi:10.1016/j.earscirev.2007.10.002

Hooke, R. L., and Iverson, R. (1995). Grain-size distribution in deforming subglacial tills: Role of grain fracture. *Geology* 23, 57–60. doi:10.1130/0091-7613(1995)023<0057:GSDIDS>2.3.CO;2

Hsü, K. J. (1975). Catastrophic debris streams (sturzstroms) generated by rockfalls. *Bull. Geol. Soc. Am.* 86 (1), 129–140. doi:10.1130/0016-7606(1975)86<129:CDSSGB>2.0.CO;2

Hu, Y., Li, H., Qi, S., Fan, G., and Zhou, J. (2020). Granular effects on depositional processes of debris avalanches. *KSCE J. Civ. Eng.* 24, 1116–1127. doi:10.1007/s12205-020-1555-3

Hungr, O. (2002). "Rock avalanche occurrence, process and modelling," in *Landslides from massive rock slope failure*. Editors S. Evans, G. Scarascia-Mugnozza, A. Strom, and R. Hermanns (Dordrecht: Springer), 285–304.

Hürlimann, M., Garcia-Piera, J. O., and Ledesma, A. (2000). Causes and mobility of large volcanic landslides: Application to tenerife, canary islands. *J. Volcanol. Geotherm. Res.* 103, 121–134. doi:10.1016/S0377-0273(00)00219-5

Hürlimann, M., Ledesma, A., and Martí, J. (1999). Conditions favouring catastrophic landslides on tenerife (canary islands). *Terra Nov.* 11, 106–111. doi:10.1046/j.1365-3121.1999.00233.x

Ibbeken, H., and Schleyer, R. (1986). Photo-sieving: A method for grain-size analysis of coarse-grained, unconsolidated bedding surfaces. *Earth Surf. Process. Landforms* 11, 59–77. doi:10.1002/esp.3290110108

Ibbeken, H., Warnke, D. A., and Diepenbroek, M. (1998). Granulometric study of the Hanaupah fan, Death Valley, California. *Earth Surf. Process. Landforms* 23, 481–492. doi:10.1002/(SICI)1096-9837(199806)23:6<481::AID-ESP906>3.0.CO;2-T

Iverson, R., and Denlinger, R. P. (2001). Flow of variably fluidized granular masses across three-dimensional terrain: 1. Coulomb mixture theory. *J. Geophys. Res. Solid Earth* 106, 537–552. doi:10.1029/2000JB900329

Iverson, R., Logan, M., and Denlinger, R. P. (2004). Granular avalanches across irregular three-dimensional terrain: 2. Experimental tests. *J. Geophys. Res. Earth Surf.* 109, 1–16. doi:10.1029/2003jf000084

Iverson, R. (1997). The physics of debris flows. *Rev. Geophys.* 35, 245–296. doi:10.1029/97RG00426

Johnson, B. C. (1978). "Blackhawk landslide, California, U.S.A," in *Rockslides and avalanches, 1. Natural phenomena*. Editor B. Voight (Pennsylvania, U.S.A: The Pennsylvania State University), 481–504. doi:10.1016/B978-0-444-41507-3.50022-2

Johnson, B. C., Campbell, C. S., and Melosh, J. H. (2016). The reduction of friction in long runout landslides as an emergent phenomenon. *J. Geophys. Res. Earth Surf.* 121, 881–889. doi:10.1002/2015jf003751

Kellerhals, R., and Bray, D. I. (1971). Sampling procedures for coarse fluvial sediments. *J. Hydraul. Div.* 97, 1165–1180. doi:10.1061/jyceaj.0003044

Legros, F. (2002). The mobility of long-runout landslides. *Eng. Geol.* 63, 301–331. doi:10.1016/S0013-7952(01)00090-4

Leyrit, H. (2000). "Flank collapse and debris avalanche deposits," in *Volcaniclastic rocks from magmas to sediments*. Editors H. Leyrit and C. Montenat (Oxfordshire, England: Routledge), 111–129.

Longchamp, C., Abellan, A., Jaboyedoff, M., and Manzella, I. (2016). 3-D models and structural analysis of rock avalanches: The study of the deformation process to better understand the propagation mechanism. *Earth Surf. Dyn.* 4, 743–755. doi:10.5194/esurf-4-743-2016

Magnarini, G., Mitchell, T. M., Goren, L., Grindrod, P. M., and Browning, J. (2021). Implications of longitudinal ridges for the mechanics of ice-free long runout landslides. *Earth Planet. Sci. Lett.* 574, 117177. doi:10.1016/j.epsl.2021.117177

Mair, K., and Hazzard, J. F. (2007). Nature of stress accommodation in sheared granular material: Insights from 3D numerical modeling. *Earth Planet. Sci. Lett.* 259, 469–485. doi:10.1016/j.epsl.2007.05.006

Makris, S., Manzella, I., Cole, P., and Roverato, M. (2020). Grain size distribution and sedimentology in volcanic mass-wasting flows: implications for propagation and mobility. *Int. J. Earth Sci.* 109, 2679–2695. doi:10.1007/s00531-020-01907-8

Makris, S., Roverato, M., Lomoschitz, A., Cole, P., and Manzella, I. (2023). The propagation and emplacement mechanisms of the Tenteniguada volcanic debris avalanche (Gran Canaria): Field evidence for brittle fault-accommodated spreading. *J. Volcanol. Geotherm. Res.* 435C, 107773. doi:10.1016/j.jvolgeores.2023.107773

Manzella, I., and Labiouse, V. (2013). Empirical and analytical analyses of laboratory granular flows to investigate rock avalanche propagation. *Landslides* 10, 23–36. doi:10.1007/s10346-011-0313-5

Manzella, I., and Labiouse, V. (2008). Qualitative analysis of rock avalanches propagation by means of physical modelling of non-constrained gravel flows. *Rock Mech. Rock Eng.* 41, 133–151. doi:10.1007/s00603-007-0134-y

Manzella, I., Penna, I., Kelfoun, K., and Jaboyedoff, M. (2016). High-mobility of unconstrained rock avalanches: Numerical simulations of a laboratory experiment and an Argentinian event. Available at: http://www.scopus.com/inward/record.url?eid=2-s2.0-84984848190&partnerID=MN8TOARS.

Martí, J., Hürlimann, M., Ablay, G. J., and Gudmundsson, A. (1997). Vertical and lateral collapses on Tenerife (Canary Islands) and other volcanic ocean islands: Comment. *Geology* 26, 861–862. doi:10.1130/0091-7613(1998)026<0861:VALCOT>2.3.CO;2

Martí, J., Soriano, C., Galindo, I., and Cas, R. A. F. (2010). Resolving problems with the origin of Las Cañadas caldera (tenerife, Canary Islands): Los Roques de García Formation-part of a major debris avalanche or an *in situ*, stratified, edifice-building succession? *Spec. Pap. Geol. Soc. Am.* 464, 113–132. doi:10.1130/2010.2464(06

Masson, D. G., Watts, A. B., Gee, M. J. R., Urgeles, R., Mitchell, N. C., Le Bas, T. P., et al. (2002). Slope failures on the flanks of the Western Canary Islands. *Earth-Science Rev.* 57, 1–35. doi:10.1016/s0012-8252(01)00069-1

Mehl, K. W., and Schmincke, H. U. (1999). Structure and emplacement of the Pliocene Roque Nublo debris avalanche deposit, Gran Canaria, Spain. *J. Volcanol. Geotherm. Res.* 94, 105–134. doi:10.1016/S0377-0273(99)00100-6

Melosh, H. J. (1979). Acoustic fluidization: a new geologic process? *J. Geophys. Res.* 84, 7513–7520. doi:10.1029/JB084iB13p07513

Melosh, H. J. (2015). Acoustic fluidization: what it is, and is not. *Bridg. Gap III Impact Cratering Nat. Exp. Model.* 1861, 1004.

Merico, A., Iezzi, G., Pace, B., Ferranti, L., Cremona, M., Scafa, M., et al. (2020). Grain size and grain size distribution of a lithified fault core in carbonates rocks using multi-scale image analysis: The example of the San Benedetto-Gioia dei Marsi fault (Central Italy). *J. Struct. Geol.* 134, 104017. doi:10.1016/j.jsg.2020.104017

Ogawa, S. (1978). "Multitemperature theory of granular materials," in *Proceedings of the U.S.-Japan seminar on continuum mechanical and statistical approaches in the mechanics of granular materials* (Sendai, Japan: U.S.-Japan Seminar), 208–217.

Paguican, E. M., Roverato, M., and Yoshida, H. (2021). "Volcanic Debris Avalanche Transport and Emplacement Mechanisms," in *Volcanic debris avalanches: From collapse to hazard*. Editors M. Roverato, A. Dufresne, and J. Procter (Heidelberg, Germany: Springer book series advances in volcanology), 143–173. doi:10.1007/978-3-030-57411-6_7

Paguican, E. M. R., (2012). The structure, morphology, and surface texture of debris avalanchedeposits: field and remote sensing mapping and analogue modelling. Dissertation, Clermont-Ferrand: Université Blaise Pascal

Palmer, B., Alloway, B., and Vincent, N. (1991). Volcanic-Debris-Avalanche Deposits in New Zealand—Lithofacies Organization in Unconfined, Wet-Avalanche Flows. *Sediment. Volcan. Settings* 1991, 89–98. doi:10.2110/pec.91.45.0089

Perinotto, H., Schneider, J. L., Bachèlery, P., Le Bourdonnec, F. X., Famin, V., and Michon, L. (2015). The extreme mobility of debris avalanches: A new model of transport mechanism. *J. Geophys. Res. Solid Earth*. 120, 8110–8119. doi:10.1002/2015JB011994

Pierson, T. C., and Costa, J. E. (1987). A rheologic classification of subaerial sediment-water flows. *GSA Rev. Eng. Geol.* 7, 1–12. doi:10.1130/REG7-p1

Pollet, N., and Schneider, J. L. M. (2004). Dynamic disintegration processes accompanying transport of the Holocene Flims sturzstrom (Swiss Alps). *Earth Planet. Sci. Lett.* 221, 433–448. doi:10.1016/S0012-821X(04)00071-8

Pudasaini, S. P., and Hutter, K. (2007). *Avalanche dynamics: Dynamics of rapid flows of dense granular avalanches*. Heidelberg, Germany: Springer Science & Business Media.

Rait, K. L., and Bowman, E. T. (2016). Influences of strain rate and shear rate on the propagation of large scale rock avalanches. *Landslides Eng. Slopes. Exp. Theory Pract.* 3, 1707–1714. doi:10.1201/b21520-212

Reubi, O., and Hernandez, J. (2000). Volcanic debris avalanche deposits of the upper Maronne valley (Cantal Volcano, France): Evidence for contrasted formation and transport mechanisms. *J. Volcanol. Geotherm. Res.* 102, 271–286. doi:10.1016/S0377-0273(00)00191-8

Roberti, G., Friele, P., van Wyk de Vries, B., Ward, B., Clague, J. J., Perotti, L., et al. (2017). Rheological evolution of the mount meager 2010 debris avalanche, southwestern British columbia. *Geosphere* 13, 369–390. doi:10.1130/GES01389.1

Roche, O., Gilbertson, M. A., Phillips, J. C., and Sparks, R. S. J. (2006). The influence of particle size on the flow of initially fluidised powders. *Powder Technol.* 166, 167–174. doi:10.1016/j.powtec.2006.05.010

Roverato, M., and Capra, L., (2013). Características microtexturales como indicadores del transporte y emplazamiento de dos depósitos de avalancha de escombros del Volcán de Colima (México. *Revista mexicana de ciencias geológicas* 30 (3), 512–525

Roverato, M., Capra, L., Sulpizio, R., and Norini, G. (2011). Stratigraphic reconstruction of two debris avalanche deposits at Colima Volcano (Mexico): Insights into pre-failure conditions and climate influence. *J. Volcanol. Geotherm. Res.* 207, 33–46. doi:10.1016/j.jvolgeores.2011.07.003

Roverato, M., Cronin, S., Procter, J., and Capra, L. (2015). Textural features as indicators of debris avalanche transport and emplacement, Taranaki volcano. *Bull. Geol. Soc. Am.* 127, 3–18. doi:10.1130/B30946.1

Roverato, M., and Dufresne, A., (2021). Volcanic debris avalanches: introduction and book structure). *Volcanic Debris Avalanches: From Collapse to Hazard*, 1–10.

Roverato, M., Larrea, P., Casado, I., Mulas, M., Béjar, G., and Bowman, L. (2018). Characterization of the Cubilche debris avalanche deposit, a controversial case from the northern Andes, Ecuador. *J. Volcanol. Geotherm. Res.* 360, 22–35. doi:10.1016/j.jvolgeores.2018.07.006

Sammis, C. G., and King, G. C. P. (2007). Mechanical origin of power law scaling in fault zone rock. *Geophys. Res. Lett.* 34, L04312. doi:10.1029/2006gl028548

Sammis, C., King, G., and Biegel, R. (1987). The kinematics of gouge deformation. *Pure Appl. Geophys. PAGEOPH* 125, 777–812. doi:10.1007/BF00878033

Schneider, J. L., and Fisher, R. V. (1998). Transport and emplacement mechanisms of large volcanic debris avalanches: evidence from the northwest sector of Cantal Volcano (France). *J. Volcanol. Geotherm. Res.* 83, 141–165. doi:10.1016/S0377-0273(98)00016-X

Scott, K., Macias, J. L., Naranjo, J. A., Rodriguez, S., and McGeehin, J. P., (2001). *Catastrophic debris flows transformed from landslides in volcanic terrains: mobility, hazard assessment, and mitigation strategies (No. 1630)*, US Department of the Interior, US Geological Survey. Available at: http://www.scopus.com/scopus/inward/record.url?eid=2-s2.0-0003273447&partner=40&rel=R4.5.0

Shea, T., van Wyk de Vries, B., and Pilato, M. (2008). Emplacement mechanisms of contrasting debris avalanches at Volcán Mombacho (Nicaragua), provided by structural and facies analysis. *Bull. Volcanol.* 70, 899–921. doi:10.1007/s00445-007-0177-7

Shea, T., and van Wyk de Vries, B. (2008). Structural analysis and analogue modeling of the kinematics and dynamics of rockslide avalanches. *Geosphere* 4, 657–686. doi:10.1130/GES00131.1

Shreve, R. L. (1968). The Blackhawk Landslide. *Geol. Soc. Am. Spec. Pap.* 108.

Shugar, D. H., and Clague, J. J. (2011). The sedimentology and geomorphology of rock avalanche deposits on glaciers. *Sedimentology* 58, 1762–1783. doi:10.1111/j.1365-3091.2011.01238.x

Siebert, L., Begét, J. E., and Glicken, H. (1995). The 1883 and late-prehistoric eruptions of Augustine volcano, Alaska. *J. Volcanol. Geotherm. Res.* 66, 367–395. doi:10.1016/0377-0273(94)00069-S

Siebert, L. (1984). Large volcanic debris avalanches: Characteristics of source areas, deposits, and associated eruptions. *J. Volcanol. Geotherm. Res.* 22, 163–197. doi:10.1016/0377-0273(84)90002-7

Siebert, L., and Roverato, M. (2021). "A Historical Perspective on Lateral Collapse and Volcanic Debris Avalanches," in *Volcanic debris avalanches: From collapse to hazard*. Editors M. Roverato, A. Dufresne, and J. Procter (Heidelberg, Germany: Springer book series advances in volcanology), 11–50.

Smyth, M. (1991). *Movement and emplacement mechanisms of the rio pita volcanic debris avalanche and its role in the evolution of Cotopaxi Volcano*. Michigan, United States: ProQuest.

Spychala, Y. T., Ramaaker, T. A., Eggenhuisen, J. T., Grundvag, S.-A., Pohl, F., and Wroblewska, S. (2021). Proximal to distal grain-size distribution of basin-floor lobes: A study from the Battfjellet Formation, Central Tertiary Basin, Svalbard. *Depos. Rec.* 0, 436–456. doi:10.1002/dep2.167

Takarada, S., Ui, T., and Yamamoto, Y. (1999). Depositional features and transportation mechanism of valley-filling Iwasegawa and Kaida debris avalanches, Japan. *Bull. Volcanol.* 60, 508–522. doi:10.1007/s004450050248

TEIDE GROUP (1997). Morphometric interpretation of the northwest and southeast slopes of Tenerife, Canary Islands. *J. Geophys. Res. Ser.* 102, 20–325.

Thompson, N., Bennett, M. R., and Petford, N. (2009). Analyses on granular mass movement mechanics and deformation with distinct element numerical modeling: Implications for large-scale rock and debris avalanches. *Acta Geotech.* 4, 233–247. doi:10.1007/s11440-009-0093-4

Thompson, N., Bennett, M. R., and Petford, N. (2010). Development of characteristic volcanic debris avalanche deposit structures: New insight from distinct element simulations. *J. Volcanol. Geotherm. Res.* 192, 191–200. doi:10.1016/j.jvolgeores.2010.02.021

Tost, M., Cronin, S. J., and Procter, J. N. (2014). Transport and emplacement mechanisms of channelised long-runout debris avalanches, Ruapehu volcano, New Zealand. *Bull. Volcanol.* 76, 881–914. doi:10.1007/s00445-014-0881-z

Ui, T. (1989). *Discrimination between debris avalanches and other volcaniclastic deposits*. Heidelberg, Germany: Springer book series advances in volcanology, 201–209. doi:10.1007/978-3-642-73759-6_13

Ui, T., and Glicken, H. (1986). Internal structural variations in a debris-avalanche deposit from ancestral Mount Shasta, California, USA. *Bull. Volcanol.* 48, 189–194. doi:10.1007/BF01087673

Ui, T. (1983). Volcanic dry avalanche deposits - Identification and comparison with nonvolcanic debris stream deposits. *J. Volcanol. Geotherm. Res.* 18, 135–150. doi:10.1016/0377-0273(83)90006-9

van Wyk de Vries, B., and Delcamp, A. (2015). *Volcanic debris avalanches*. Amsterdam, Netherlands: Elsevier Inc. doi:10.1016/B978-0-12-396452-6.00005-7

van Wyk De Vries, B., Self, S., Francis, P. W., and Keszthelyi, L. (2001). A gravitational spreading origin for the Socompa debris avalanche. *J. Volcanol. Geotherm. Res.* 105, 225–247. doi:10.1016/S0377-0273(00)00252-3

Vezzoli, L., Apuani, T., Corazzato, C., and Uttini, A. (2017). Geological and geotechnical characterization of the debris avalanche and pyroclastic deposits of Cotopaxi Volcano (Ecuador). A contribute to instability-related hazard studies. *J. Volcanol. Geotherm. Res.* 332, 51–70. doi:10.1016/j.jvolgeores.2017.01.004

Voight, B., Janda, R. J., Glicken, H., and Douglass, P. M. (1983). Nature and mechanics of the Mount St Helens rockslide-avalanche of 18 May 1980. *Geotechnique* 33, 243–273. doi:10.1680/geot.1983.33.3.243

Voight, B., Komorowski, J. C., Norton, G. E., Belousov, A. B., Belousova, M., Boudon, G., et al. (2002). The 26 December (Boxing Day) 1997 sector collapse and debris avalanche at Soufrière Hills Volcano, Montserrat. *Geol. Soc. Mem.* 21, 363–407. doi:10.1144/GSL.MEM.2002.021.01.17

Walter, T. R., Haghshenas Haghighi, M., Schneider, F. M., Coppola, D., Motagh, M., Saul, J., et al. (2019). Complex hazard cascade culminating in the Anak Krakatau sector collapse. *Nat. Commun.* 10, 4339. doi:10.1038/s41467-019-12284-5

Wang, Y. F., Cheng, Q. G., Shi, A. W., Yuan, Y. Q., Yin, B. M., and Qiu, Y. H. (2019). Sedimentary deformation structures in the Nyixoi Chongco rock avalanche: implications on rock avalanche transport mechanisms. *Landslides* 16, 523–532. doi:10.1007/s10346-018-1117-7

Yang, Q., Su, Z., Cai, F., and Ugai, K. (2015). Enhanced mobility of polydisperse granular flows in a small flume. *Geoenvironmental Disasters* 2, 12. doi:10.1186/s40677-015-0019-4

Zhang, M., and McSaveney, M. J. (2017). Rock avalanche deposits store quantitative evidence on internal shear during runout. *Geophys. Res. Lett.* 44, 8814–8821. doi:10.1002/2017GL073774

Zhang, W., Wang, Q., Chen, J., Li, H., Que, J., and Kong, Y. (2015). Grain-size analysis of debris flow alluvial fans in Panxi area along Jinsha River, China. *Sustainability* 7, 15219–15242. doi:10.3390/su71115219